Boundary-Layer Meteorol (2017) 164:217–247
DOI 10.1007/s10546-017-0245-2

RESEARCH ARTICLE

Comprehensive Evaluation of Fast-Response, Reynolds-Averaged Navier–Stokes, and Large-Eddy Simulation Methods Against High-Spatial-Resolution Wind-Tunnel Data in Step-Down Street Canyons

Arash Nemati Hayati[1] · Rob Stoll[1] · J. J. Kim[2] · Todd Harman[1] · Matthew A. Nelson[3] · Michael J. Brown[3] · Eric R. Pardyjak[1]

Received: 26 July 2016 / Accepted: 9 March 2017 / Published online: 18 May 2017

Abstract Three computational fluid dynamics (CFD) methods with different levels of flow-physics modelling are comprehensively evaluated against high-spatial-resolution wind-tunnel velocity data from step-down street canyons (i.e., a short building downwind of a tall building). The first method is a semi-empirical fast-response approach using the Quick Urban Industrial Complex (QUIC-URB) model. The second method solves the Reynolds-averaged Navier–Stokes (RANS) equations, and the third one utilizes a fully-coupled fluid-structure interaction large-eddy simulation (LES) model with a grid-turbulence inflow generator. Unlike typical point-by-point evaluation comparisons, here the entire two-dimensional wind-tunnel dataset is used to evaluate the dynamics of dominant flow topological features in the street canyon. Each CFD method is scrutinized for several geometric configurations by

✉ Eric R. Pardyjak
pardyjak@mech.utah.edu

Arash Nemati Hayati
a.nematihayati@utah.edu

Rob Stoll
rstoll@eng.utah.edu

J. J. Kim
jjkim@pknu.ac.kr

Todd Harman
t.harman@utah.edu

Matthew A. Nelson
nelsonm@lanl.gov

Michael J. Brown
mbrown@lanl.gov

1 Department of Mechanical Engineering, University of Utah, Salt Lake City, UT 84112, USA

2 Department of Environmental Atmospheric Sciences, Pukyong National University, Busan, South Korea

3 Los Alamos National Laboratory, Information Systems and modelling Group, Los Alamos, NM 87545, USA

varying the downwind-to-upwind building-height ratio (H_d/H_u) and street canyon-width to building-width aspect ratio (S/W) for inflow winds perpendicular to the upwind building front face. Disparities between the numerical results and experimental data are quantified in terms of their ability to capture flow topological features for different geometric configurations. Overall, all three methods qualitatively predict the primary flow topological features, including a saddle point and a primary vortex. However, the secondary flow topological features, namely an in-canyon separation point and secondary vortices, are only well represented by the LES method despite its failure for taller downwind building cases. Misrepresentation of flow-regime transitions, exaggeration of the coherence of recirculation zones and wake fields, and overestimation of downwards vertical velocity into the canyon are the main defects in QUIC-URB, RANS and LES results, respectively. All three methods underestimate the updrafts and, surprisingly, QUIC-URB outperforms RANS for the streamwise velocity component, while RANS is superior to QUIC-URB for the vertical velocity component in the street canyon.

Keywords Flow topology · Large-eddy simulation · Reynolds-averaged Navier–Stokes · Street-canyon flow

1 Introduction

The urban micro-climate plays an important role in the transport of pollutants, energy and water use, and in the transport of momentum (Wu and Kriksic 2012). These transport processes are modified by a myriad of factors including: large-scale meteorological processes, urban morphology, vegetation cover, and water resource management (Hang et al. 2009; Shishegar 2013). The impacts of these factors on the surrounding environment have been the focus of numerous research (Arnfield 2003; Collier 2006; Souch and Grimmond 2006; Moonen et al. 2012). Despite the critical role of field and laboratory experiments in urban micro-climate research, the scarcity of experimental data over full urban domains and the difficulty of acquiring detailed turbulent flow statistics make numerical methods an attractive option for studying urban fluid mechanics (Fernando et al. 2001; Blocken and Stathopoulos 2013; Blocken 2015). A recent literature review (Singh and Laefer 2015) indicates an increased reliance on numerical modelling compared with wind-tunnel or field measurements in wind environment, air quality, and urban-heat island research.

For the last three decades, computational fluid dynamics (CFD) methods have been used extensively to examine the intricacies of urban-flow structures (Murakami et al. 1999; Britter and Hanna 2003; Britter and Schatzmann 2007; Salim and Ong 2013). Urban CFD applications include pedestrian comfort, plume transport, building energy consumption, and natural ventilation (Toparlar et al. 2015). CFD is also utilized in urban design to study the impacts of diverse architectural forms on local airflow characteristics, including flow separation points and vortex cores (Chung and Malone-Lee 2010). We refer to CFD methods as any approach that solves the fundamental transport equations on a gridded domain. Typical CFD methods employed for the analysis of urban flows may be classified into three main categories, each having different levels of physical representation and computational requirements, namely: (1) fast-response (or simplified CFD, see e.g., Kochanski et al. 2015), (2) Reynolds-averaged Navier–Stokes (RANS), and (3) large-eddy simulation (LES). While other promising approaches exist, such as detached-eddy simulation (Liu and Niu 2016), we focus here on the three most widely used methods.

Fast-response urban flow and dispersion models provide results for quick turn-around applications such as the rapid estimation of toxic chemical dispersion, training exercises, or where large numbers of simulations must be performed in a short period of time (e.g., Brown et al. 2013; Kochanski et al. 2015). The Plume Rise Model Enhancement fast-response urban-flow model is one example (Schulman et al. 2000), and uses experimental data to compute velocity and turbulence fields around isolated buildings. Other fast-response urban-flow models take an additional step and require that the velocity field computed from empirical models also adheres to conservation of mass. Examples of these mass-consistent models include the Quick Urban Industrial Complex flow solver QUIC-URB (Singh et al. 2008), Ausbreitungs-und Stromungs-Modell fur Urbane Strukturen (Gross 1997), and Micro-Swift-Spray (Tinarelli et al. 2007).

RANS solvers compute flow solutions to the ensemble-averaged Navier–Stokes equations using a turbulence closure model for the Reynolds shear stress (Wilcox 2006). This method has been investigated for a range of urban configurations, including isolated buildings (Tominaga et al. 2008; Tominaga and Stathopoulos 2010), idealized urban canopies (Alegrini et al. 2014), semi-idealized canopies (Hertwig et al. 2012) and full-scale field experiments (Blocken and Persoon 2009; Janssen et al. 2013).

The LES technique computes solutions to the filtered Navier–Stokes equations. It resolves large-scale energetic turbulent motions, while using a subgrid-scale model to represent unresolved motions, giving LES the ability to represent unsteady phenomena in complex urban terrain. The capability of modelling fluctuations and periodic motions is a noticeable benefit over other methods in urban flows (Murakami 1997; Tominaga and Stathopoulos 2011; Salim et al. 2011). However, due to computational resource limitations, fewer LES studies have been carried out on the urban micro-climate compared with other numerical approaches (Blocken and Stathopoulos 2013).

Using the above-mentioned CFD approaches, numerous investigations have focused on flow in idealized street canyons, which are the fundamental building units of urban infrastructure. Studies have revealed the impact of building geometry on vortex formation and plume concentration in idealized street canyons (Xie et al. 2005). However, CFD simulations have failed to reproduce the correct level of vortex intensity and the correct sign and magnitude of the vertical velocity component inside the canyon (Santiago et al. 2007). These deficiencies were mostly due to incorrect momentum transport (Ketzel et al. 2000; Sahm et al. 2002), and the underestimation of turbulence intensity and air ventilation from intersecting streets (Neofytou et al. 2008).

Despite the existence of many CFD studies, there are three significant aspects that have rarely been addressed in street-canyon analysis. First, most were limited to simple idealized street canyons with isolated or single-height building configurations. Second, the sensitivity of spatial-flow-structure patterns to changes in the street-canyon geometry was not addressed. Finally, the evaluation process was mostly based on a restricted point-by-point comparison of the velocity field, and has lacked continuous high-spatial-resolution wind-tunnel data (Addepalli and Pardyjak 2015). Considering the geometric variability of street canyons in real cities, numerical approaches have not been sufficiently examined for their ability to reproduce dominant flow topological features with respect to experimental data (Koutsourakis et al. 2012). Thus, the comprehensive evaluation of CFD methods for more complex idealized street-canyon geometries, such as step-down street canyons (i.e., a short building downwind of a tall building), is an important step towards reliable CFD usage in urban-flow studies. Further, the reproduction of various flow intricacies and dominant flow topological features, including the primary and secondary vortex, saddle point and the in-canyon separation point is needed.

Here, we investigate the intricacies of flow patterns in idealized street canyons of uneven building heights using CFD with different flow physics. We compare the numerical results with each other and against experimental data for step-down street canyons defined by their downwind-to-upwind building-height ratio ($H_d/H_u < 1$), where the height of the upwind building (H_u) is greater than the downwind building height (H_d). We compare and assess the momentum field in step-down street canyons computed from fast-response, RANS and LES methods against published high-spatial-resolution wind-tunnel particle-imaging velocimetry (PIV) data (Addepalli and Pardyjak 2015), focusing on the reproduction of diverse flow structures, and flow-structure transitions existing in step-down street canyons (e.g., rooftop recirculation zones, street-canyon cavities, building sidewall and downwind wake patterns and vertical advection). Specifically, we vary the downwind-to-upwind building-height ratio and canyon-length to building-width aspect ratio (S/W, where S is the length of the street canyon and W is the width of the building). We also scrutinize the prediction of major flow topological features (i.e., primary vortex, secondary recirculation zone, saddle point and in-canyon separation streamline), and examine how each model predicts changes in flow topological features with variations of H_d/H_u and S/W. Finally, we quantitatively examine the prediction of streamwise and vertical velocity components throughout the entire canyon by the different methods.

2 Model Description

2.1 QUIC-URB

QUIC-URB is a fast-response simplified CFD model based on the concept proposed by Rockle (1990); it uses a three-dimensional mass-consistent approach to compute temporally-averaged wind fields around explicitly resolved individual buildings. An initial wind field ($\vec{V_o} = u_o\hat{i} + v_o\hat{j} + w_o\hat{k}$) is generated based on empirical parametrizations for urban-flow structures, including upwind and downwind cavities, rooftop recirculation zones, street canyons and street intersections (see Singh et al. 2008; Gowardhan et al. 2010; Brown et al. 2013). After computing $\vec{V_o}$ according to the parametrizations, the velocity field is forced to be mass consistent subject to the weak constraint that the variance of the difference between the initial and final velocity fields ($\vec{V_o}$ and $\vec{V}$, respectively) is minimized. QUIC-URB has been evaluated against wind measurements and point-source-release tracer measurements in the business districts of Salt Lake City (Gowardhan et al. 2006), Oklahoma City (Neophytou et al. 2011; Brown et al. 2013), and New York City (NYC), where QUIC-URB performed as well as a suite of five different CFD codes in blind tests based on standard plume-modelling statistical comparisons (Allwine et al. 2008). QUIC-URB is among the most published urban fast-response mass-conserving three-dimensional wind solvers. Since 2006, the fidelity of QUIC-URB has been extensively discussed and examined for urban applications (Gowardhan et al. 2006; Singh et al. 2008; Hanna et al. 2011; Neophytou et al. 2011; Brown et al. 2013; Kochanski et al. 2015; Nelson et al. 2016).

We use the QUIC-URB model version 6.01, which includes a new parametrization for the sidewall-wake recirculation zones around buildings (Sect. 2.1.1). Compared with previous versions of the QUIC-URB model (not shown here for brevity), the new parametrization significantly improves the representation of sidewall-wake flow patterns, vertical flow motions and the flow patterns in the upper half of the street canyon.

2.1.1 QUIC-URB Sidewall Recirculation Algorithm

A new parametrization in QUIC-URB version 6.01 that has not yet been described is the sidewall algorithm, which is applied after the upwind recirculation, downwind wake, and street-canyon algorithms are also applied to the building. Horizontally-rotating sidewall vortices are produced in the low pressure regions that develop due to separated flow occurring on either side of the front wall as the flow is diverted laterally around the front face of the building (Hosker 1984).

Due to this directional dependence of the sidewall vortex formation, the sidewall algorithm first checks the relative angle between the local wind vector and the faces of the building. Vortices are formed only when a face has an outward normal vector nominally ($\pm 10°$) perpendicular to the local wind vector, and the outward normal vector of the upwind adjacent sidewall face is nominally ($\pm 10°$) parallel to the local wind vector. For an idealized building with a rectangular footprint, this is done with a single check of the relative angle between the local wind vector and the building rotation angle. For buildings with an arbitrary polygon footprint, each face must be checked individually.

The sidewall vortex algorithm checks for the influence of other building flow algorithms on the upwind edge of the sidewall, and does not place a sidewall vortex at the vertical level where a wake field or street-canyon flow algorithm from an upwind building has been applied. This on/off switch is designed to simulate the interruption of the strong lateral flow by more dominant flow structures upwind. At the vertical levels where the sidewall algorithm is utilized, the vortex is defined similar to QUIC-URB's rooftop vortex that develops along the upwind edge of a flat roof and nominally perpendicular to the prevailing flow direction (Wilson 1979; Pol et al. 2006; Singh et al. 2008). The important parameters controlling the sidewall vortex strength and geometry are

$$R = B_s^{2/3} B_l^{1/3}, \tag{1a}$$

$$L_c = 0.9R, \tag{1b}$$

$$W_c = 0.22R, \tag{1c}$$

where B_s is the smaller of the height (H) and the effective cross-wind width (W_{eff}) of the building (Nelson et al. 2008), B_l is the larger of H and W_{eff}, R is the vortex size scaling factor, L_c is the downwind length of the half-ellipse that defines the vortex recirculation region, and W_c is the lateral width of the elliptical recirculation region. A reference velocity (U_0) is chosen from the undisturbed profile at the vertical level in question to scale the velocities within the elliptical recirculation zone, and is specified as the velocity at the edge of the external boundary layer growing from the leading edge of the sidewall and propagating downstream of the encompassing recirculation region. Within the recirculation zone, the velocity is reversed and scaled linearly from the reference wind speed near the wall to zero at the edge of the ellipse.

2.2 Reynolds-Averaged Navier–Stokes

The RANS method of Kim and Baik (2010) used here assumes a three-dimensional, non-hydrostatic, non-rotating, and Boussinesq airflow system, together with the renormalization group (RNG) k–ε turbulence closure. The thermodynamic energy equation is not taken into account owing to the isothermal conditions. For properly representing the effects of the wall boundaries, the turbulent wall function of Versteeg and Malalasekera (1995) is implemented to avoid the computational costs of resolving the details of the near-wall turbulent flow. Com-

parison with the experimental data of Uehara et al. (2000) suggests the chosen RANS method reliably simulates urban street-canyon flow (see Kim and Baik 2010). In general, the RNG k–ε turbulence closure model has been found to have the best agreement with experimental data in urban RANS studies (Kim and Baik 2004, 2010; Tominaga and Stathopoulos 2009, 2010; Koutsourakis et al. 2012), making it a logical choice for our comparative study.

2.3 Large-Eddy Simulation

Uintah:MPMICE has been used for a number of LES studies of street canyons and cities (Hayati et al. 2014, 2016). Uintah:MPMICE is an Eulerian–Lagrangian two-way coupled fluid-structure interaction LES code developed within a massively parallel computational framework (Germain et al. 2000; Parker et al. 2006; Parker 2006; Meng and Berzins 2014). Structural mechanics are represented using the material point method (MPM) that discretizes solids into a collection of particles (material points) with appropriately specified material properties, which account for both solid deformations and coupling to the flow field. Particle evolution is then tracked in a Lagrangian frame of reference, where particle interaction occurs through a background mesh rather than direct mutual communication. At each timestep, the background mesh is used to calculate velocity gradients from the governing equations (see Xia 2006; Guilkey et al. 2007, for further details on the MPM solver). The Implicit Continuous fluid Eulerian (ICE) solver is a multi-material Eulerian cell-centred finite-volume compressible flow solver based on Kashiwa et al. (1996) and Kashiwa (2001) in which we have implemented different LES subgrid-scale models. The multi-material formulation of the ICE solver includes two steps, namely, an Eulerian step, where conservation of mass, momentum and energy are satisfied in each cell, and then a Lagrangian step in which the contribution of the incoming and outgoing fluxes for each cell are used to update the material state of the cells. The LES non-hydrostatic, non-Boussinesq multi-material equations of conservation of mass, momentum, and energy are defined by

$$\frac{\partial \widetilde{\rho^m}}{\partial t} + \frac{\partial \widetilde{\rho^m}\widetilde{u_j}}{\partial x_j} = 0, \tag{2a}$$

$$\frac{\partial \widetilde{\rho^m}\widetilde{u_i^m}}{\partial t} + \frac{\partial \widetilde{\rho^m}\widetilde{u_i^m}\widetilde{u_j^m}}{\partial x_j} = \theta^m \frac{\partial \widetilde{\sigma_{ij}}}{\partial x_j} + \widetilde{\rho^m} g_i + \frac{\partial \theta^m (\widetilde{\sigma_{ij}^m} - \widetilde{\sigma_{ij}})}{\partial x_j} - \frac{\partial \widetilde{\rho^m}}{\partial x_j}(\widetilde{u_i^m u_j^m} - \widetilde{u_i^m}\widetilde{u_j^m}) + \sum_{l=1}^{N} \widetilde{f_i^{lm}}, \quad \text{and} \tag{2b}$$

$$\frac{\partial \widetilde{\rho^m}\widetilde{e^m}}{\partial t} + \frac{\partial \widetilde{\rho^m}\widetilde{e^m}\widetilde{u_j^m}}{\partial x_j} = -\widetilde{p}\theta^m \frac{\dot{\upsilon^m}}{\upsilon^m} + \theta^m \widetilde{\tau_{ij}} \frac{\partial \widetilde{u_i}}{\partial x_j} + \theta^m (\widetilde{\sigma_{ij}^m} - \widetilde{\sigma_{ij}}) \frac{\partial \widetilde{u_i^m}}{\partial x_j} - \frac{\partial \widetilde{\rho^m}}{\partial x_j}(\widetilde{e^m u_j^m} - \widetilde{e^m}\widetilde{u_j^m}) - \frac{\partial \widetilde{q_j^m}}{\partial x_j} + \sum_{l=1}^{N} \widetilde{E^{lm}} \tag{2c}$$

respectively. Here, g_i and x_j denote the acceleration due to gravity and spatial coordinate components, respectively, t is time, a ($\sim$) indicates the LES filtering operation, m is an index indicating different materials to which the conservation equations apply, θ^m, u^m, ρ^m, σ^m, and f_i^{lm} represent the material m volume fraction, velocity, density, total stress and momentum exchange force among different materials, respectively, and p, e^m, υ^m, $\dot{\upsilon}^m$, q^m, and E^{lm}, are pressure, internal energy, specific volume, the rate of change of specific volume, thermal flux, and the energy exchange among different materials, respectively, for a material m. The fourth

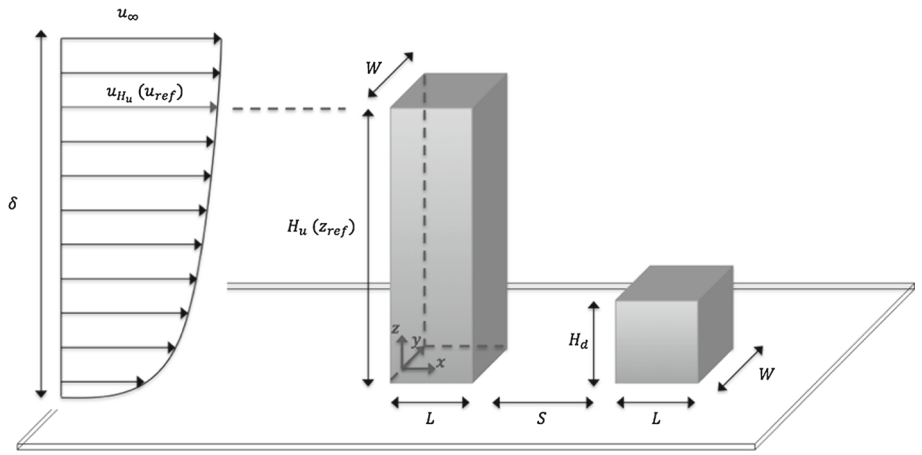

Fig. 1 Illustration of the parameters used in the step-down test cases; L building along-wind length, W building cross-wind width, S street-canyon along-wind width, $H_u(z_{ref})$: upwind building height, H_d: downwind building height, δ: boundary-layer height, u_∞: freestream velocity, $u_{H_u}(u_{ref})$: streamwise velocity component at $z = H_u$

terms on the right-hand side of Eqs. 2b and 2c represent the subgrid-scale stress and heat flux, respectively, and are modelled using the dynamic Smagorinsky model (Germano et al. 1991; Lilly 1992), which provides better results than the standard Smagorinsky model for urban-flow studies (Murakami 1998), and is one of the most commonly used LES subgrid-scale models in general. Additionally, LES results have been reported to be insensitive to the subgrid-scale model formulation for flows around buildings, since a significant portion of turbulent eddies are resolved in the computational domain (Gousseau et al. 2013) (see Xia 2006; Guilkey et al. 2007, for further details on the ICE solver). Our motivation for using a fluid-structure interaction code here is primarily its ability to handle a wide variety of environmental fluid dynamics applications (e.g., forest damage, storm, and tornado simulations) on very large computational scales. Moreover, the code facilitates the use of a new grid-turbulence inflow generator described in Sect. 4.3.

3 Canyon Configurations

Our street-canyon configurations are identical to those in Addepalli and Pardyjak (2015). Geometric and mean inflow velocity parameters defined for the step-down street-canyon cases are illustrated in Fig. 1, where W, L, S, H_u, H_d, u_∞, and u_{H_u} are the building cross-wind width, building along-wind length, street canyon along-wind width, upwind building height, downwind building height, upstream reference velocity, and streamwise velocity component at the height of the upwind building, respectively. In the figures and discussion throughout, the origin of the coordinate system is at the mid-width of the upstream building leading edge on the ground surface (Fig. 1).

The inflow profiles are shown in Fig. 2 at $4L$ upstream of the first building. The inflow formulation for the QUIC-URB and RANS models is described in Sects. 4.1 and 4.2, respectively. Note that in QUIC-URB, there is no explicit turbulence model and thus no inflow turbulence intensity (Fig. 2b). For RANS, the turbulence intensity profile was obtained based on the turbulence kinetic energy as described in Sect. 4.2. For LES, a grid-turbulence inflow

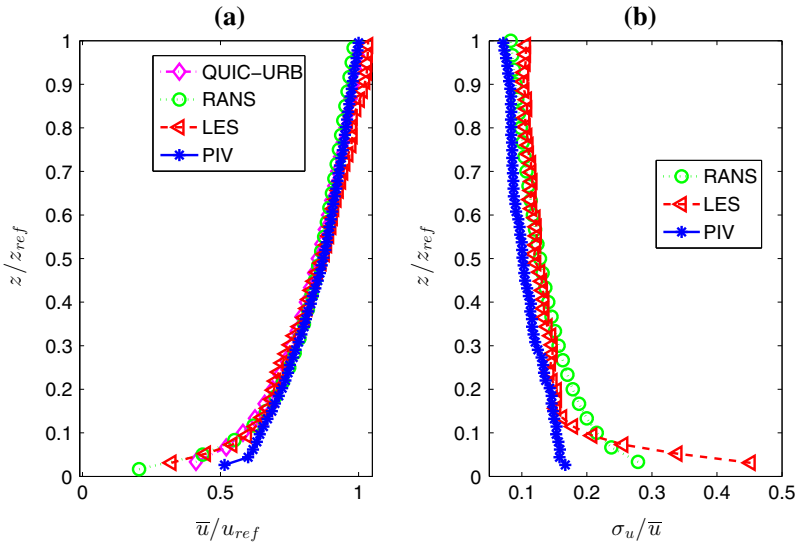

Fig. 2 Normalized inflow profiles in step-down street canyons at $4L$ upstream of the upwind building: **a** mean streamwise velocity component and **b** streamwise turbulence-intensity components. Note that $z_{\mathrm{ref}} = 121.6$ m and $u_{\mathrm{ref}} = 6.72\,\mathrm{m\,s^{-1}}$

generator simulated the appropriate level of wind shear in the mean streamwise velocity component as described in Sect. 4.3.

For all cases, the along-wind length and cross-wind width of the buildings are fixed at $W = L \approx 32$ m, and the height of the upwind building is fixed at $H_{\mathrm{u}} \approx 121.6$ m. The (downwind-to-upwind) building-height ratio ($H_{\mathrm{d}}/H_{\mathrm{u}}$) changes systematically with $H_{\mathrm{d}}/H_{\mathrm{u}} \approx 0, 0.08, 0.16, 0.26, 0.34, 0.42, 0.53, 0.61, 0.69$. For each building-height ratio, we consider two different building aspect ratios (e.g., $S/W \approx 2.5$ and 1) by varying the street-canyon along-wind width from $S \approx 80$ m (wide street canyon) to $S \approx 32$ m (narrow street canyon). In summary, for each street-canyon width, we examine eight test cases of QUIC-URB and RANS with $0.08 \leqslant H_{\mathrm{d}}/H_{\mathrm{u}} \leqslant 0.69$ and five cases of LES for $H_{\mathrm{d}}/H_{\mathrm{u}} \approx 0, 0.08, 0.27, 0.34, 0.69$.

4 Numerical Configuration

4.1 QUIC-URB

The distances to the inflow, lateral, and outflow boundaries from the buildings are $5L$, $5L$, and $10L$, respectively, and the grid spacing in the x, y, and z directions is 3.2 m (1,782,000 total cells). Further grid refinement did not significantly change the QUIC-URB results. QUIC-URB only requires the mean wind profile at the domain inlet, and we use a power-law fit to the experimental mean inflow velocity of Addepalli and Pardyjak (2015),

$$u(z) = u_{\mathrm{ref}} \left(\frac{z}{z_{\mathrm{ref}}} \right)^{a}, \tag{3}$$

where z_{ref}, u_{ref}, and a represent the reference height, streamwise velocity component at z_{ref}, and the power-law exponent, respectively. The profile of the inflow turbulence intensity is

Table 1 Main parameters for the QUIC-URB simulations

Parameter/model	Value/type
Grid spacing ($s_x \times s_y \times s_z$)	3.2 m × 3.2 m × 3.2 m
Numerical domain size ($L_x \times W_y \times H_z$)	$18L \times 11L \times 9L$
Inflow parameters	$u_{\text{ref}} = 6.72\ \text{m s}^{-1}$, $z_{\text{ref}} = 121.6$ m, $a = 0.205$
Street-canyon algorithm	Rockle with Fackrell cavity
Blended region algorithm	On
Rooftop algorithm	Recirculation
Upwind-cavity algorithm	High-rise MVP model
Wake algorithm	Area scaled
Rooftop surface roughness length (z_o)	0.1 m
Building sidewall recirculation	On

Table 2 Main parameters for the RANS simulations

Parameter/model	Value/type
Grid size ($s_x \times s_y \times s_z$)	3.2 m × 3.2 m × 3.2 m
Numerical domain size ($L_x \times W_y \times H_z$)	$18\,L \times 11\,L \times 9\,L$
Inflow parameters	$u_{\text{ref}} = 6.72\,\text{m s}^{-1}$, $z_{\text{ref}} = 121.6$ m, $a = 0.205$, $C_\mu = 0.0845$
Turbulence model	RNG k-ε
Wall function	Turbulent wall function

not defined in the QUIC-URB model since the methodology is fundamentally dependent on street-canyon parametrizations and no turbulence model is implemented. The domain height is fixed at 288 m for all test cases. The domain size, inflow parameters, and different algorithms employed in QUIC-URB are presented in Table 1.

4.2 Reynolds-Averaged Navier–Stokes

The domain size in relation to the building width, the grid resolution, and the inflow wind profile used in the RANS simulations are the same as those used for the QUIC-URB simulations (Table 2). Selected runs at higher resolution, i.e., 1.6 m × 1.6 m × 1.6 m improved numerical results negligibly. The required inflow profiles for turbulence kinetic energy (k) and its dissipation rate (ε) are specified following Apsley and Castro (1997) as

$$k(z) = \frac{1}{C_\mu^{0.5}} u_*^2 \left(1 - \frac{z}{\delta}\right)^2, \tag{4a}$$

$$\varepsilon(z) = \frac{C_\mu^{0.75} k^{1.5}}{\kappa z}, \tag{4b}$$

where u_*, κ, and C_μ are the friction velocity, von Karman constant ($\kappa = 0.4$), and empirical constant ($C_\mu = 0.0845$) in the $k - \varepsilon$ turbulence closure scheme. The streamwise component of turbulence intensity is then derived with the assumption of turbulence isotropy. A zero-gradient condition is applied at the top surface. Symmetry boundary conditions are applied at lateral surfaces, and zero static pressure is specified at the outlet.

4.3 Large-Eddy Simulation

The grid spacing in the x, y, and z directions is 2 m (3,120,000 total cells), with resolution tests on selected cases at a coarser grid spacing (3.2 m) resulting in a loss of secondary recirculation zones observed in the experimental data. Grid refinement (to 1 m) did not lead to significant improvements in the representation of features in the mean velocity field. Previous work has demonstrated that the details of LES velocity fields can be highly sensitive to turbulent inflow conditions (e.g., Tabor and Baba-Ahmadi 2010), and preliminary LES tests confirmed the strong sensitivity to inlet boundary conditions. Most existing turbulent inflow boundary conditions for LES use some variation of precursor simulation data (Munters et al. 2016), synthetic methods (Muñoz-Esparza et al. 2015), or flow rescaling (Yang and Meneveau 2016). However, these methods are computationally intensive and require the handling of large amounts of data.

A new inflow generator was thus developed using Uintah:MPMICE material points to directly place a rigid grid at the inlet of the computational domain (Fig. 3a). The concept of grid-turbulence generation has been extensively investigated in wind-tunnel studies (Comte-Bellot and Corrsin 1966; Seoud and Vassilicos 2007; Valente and Vassilicos 2011), but rarely examined numerically for LES inflow. Here, the grid-turbulence inflow generator consists of spanwise (along y) and vertical (along z) rectangular bars located at the inlet of the computational domain (Fig. 3b). Two features of the inlet profile were found to have the strongest impact on flow dynamics, mean shear and velocity profiles and turbulence intensity. The desired vertical velocity profile was created by positioning the spanwise bars with a progressive vertical spacing defined by

$$z_{K+1} = z_K + (L_i + K L_p), \tag{5}$$

where K is the index for the spanwise bars with $K = 0, 1, 2, \ldots, N$, with N the index of the last bar, z_K is the z coordinate of the centreline of the Kth bar, with $z_0 = 0$ and $z_N \leqslant \delta - \varepsilon_z$, and L_i and L_p are the initial and step-progression lengths, respectively. The vertical clearance length ε_z prevents the interference of the last bar with the top boundary of the domain. The turbulence intensity is adjusted with a set of uniform vertical bars located at

$$y_{Q+1} = y_Q + L_\mathrm{u} \tag{6}$$

where Q is the index for the vertical bars for $Q = 0, 1, 2, \ldots, M$, with M the index of the last vertical bar and y_Q is the y coordinate of the centreline of the Qth bar, with $y_0 = 0$ and $y_M \leqslant W_y - \varepsilon_y$. The spanwise clearance length ε_y prevents the grid from interfering with the lateral domain boundary, and L_u is the uniform step length. In addition to the turbulence grid, the ground surface is covered with homogeneous square-shaped surface roughness elements (Fig. 3a) to approximate the upstream wind-tunnel floor roughness elements used in the experiment (Addepalli and Pardyjak 2015). Inside the canyon, surface roughness elements are not included (Addepalli and Pardyjak 2015). The combination of the surface roughness elements and turbulence-grid results in an LES inflow profile of the streamwise component of the turbulence intensity matching the experimental data away from the wall very well, but overestimating values near the wall (Fig. 2).

The dimensions of the computational domain, inlet grid, and roughness elements are given in Table 3. The width of the inflow grid bars (W_b) is 6 m, and the length and width of the surface roughness elements (l_sr and w_sr, respectively) are both 6 m, with a height (h_sr) of 4 m. In preliminary runs, the inlet distance was varied and the velocity profile at $4L$ upstream of the first building was compared against experimental data (Fig. 2). Based on those results,

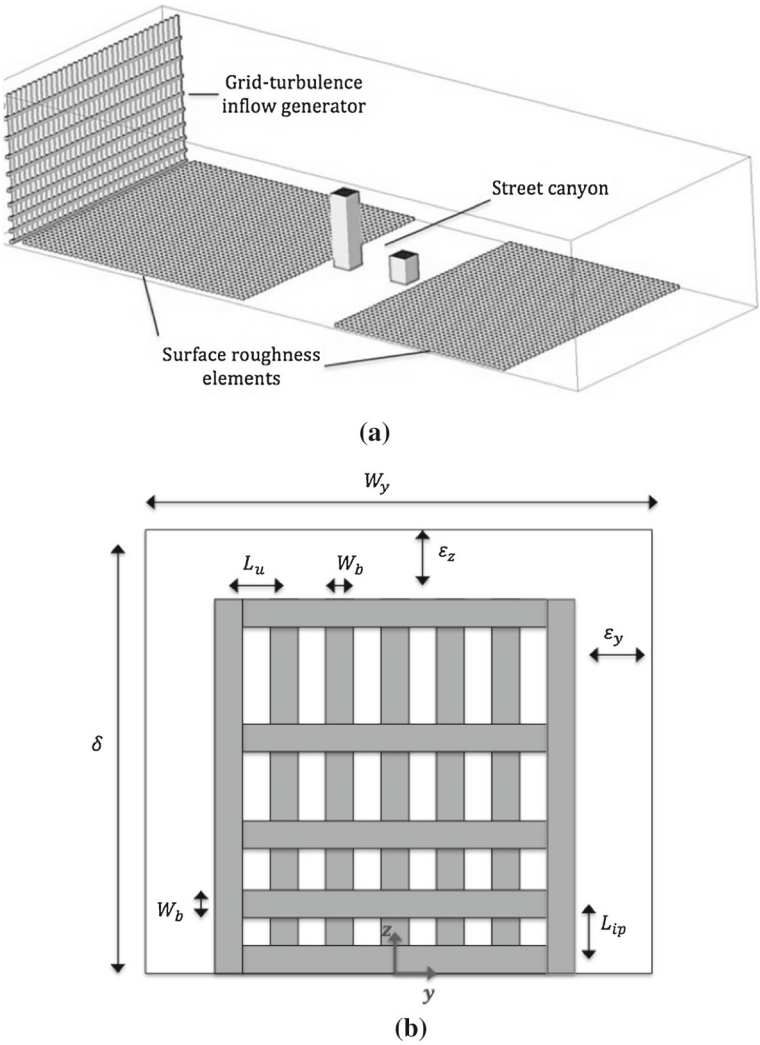

Fig. 3 LES domain set-up with the grid-turbulence inflow generator at the inlet and homogeneous square-shaped surface roughness elements covering the surroundings of the street canyon **a** overall view **b** schematic of the grid-turbulence inflow generator

we set the inlet distance to $15L$, which is a sufficient distance ($15L$ from the buildings) to allow for the mixing of the grid-turbulence structures, and to produce a sufficient level of turbulence perturbation at the inflow upstream of the buildings.

The outflow boundary conditions use the local one-dimensional inviscid boundary condition to avoid reflected wake propagation (Poinsot and Veynante 2001). The distances to the side, and outflow boundaries from the buildings are $6L$ and $17L$ ($L \approx 32$ m), respectively. The lateral domain boundaries use a symmetry condition for all prognostic variables, while the domain top surface uses a zero-gradient condition on all variables. The no-slip boundary condition is enforced at all solid surfaces via the momentum exchange term $\widetilde{f^{\mathrm{lm}}}$ in Eq. 2b.

Table 3 Main parameters for the LES simulations

Parameter/model	Value/type
Numerical domain size ($L_x \times W_y \times H_z$)	$32L \times 13L \times 7.5L$
Inflow parameters	$u_{\text{ref}} = 6.72\,\text{ms}^{-1}$, $L_i = 18\,\text{m}$, $L_\text{p} = 2$ m, $\varepsilon_z = \varepsilon_y = 2$ m, $L_\text{u} = 12$ m, $W_y = 384$ m, $W_b = l_\text{sr} = w_\text{sr} = 6$ m, $h_\text{sr} = 4$ m, $\delta = 240$ m
Subgrid-scale turbulence model	Dynamic Smagorinsky

Table 4 Computational cost for one test case simulation

Method	Number of cores	Computational time	Total computational cost (CPU hours)	Computer system
QUIC-URB	1	5 sec	0.0014	MacBook Pro 2.6 GHz Core i5
RANS	4	5 h	20	MacBook Pro 2.6 GHz Core i5
LES	480	2.5 days	28,800	NCAR and XSEDE supercomputers

4.4 Computational Cost

The computational costs for the QUIC-URB, RANS and LES methods are given in Table 4. QUIC-URB is the fastest and cheapest method, with a running time ≈5 sec on one core, followed by RANS which is completed within ≈5 h on four cores using a MacBook Pro 2.6 GHz Core i5 personal computer. LES is the most expensive method, requiring significantly more computational resources together with a much longer running time of ≈2.5 days on 480 cores of NCAR's Yellowstone and XSEDE's Stampede supercomputer clusters. The total computational cost of even a single LES simulation is over 1400 times that of a RANS simulation, while QUIC-URB is the cheapest method with a total computational cost of ≈0.0014 CPU h, or over 14,000 times cheaper than a RANS simulation.

5 Results and Discussion

In this section, we present the numerical results obtained from the three CFD methods. We compare numerical results on a vertical plane along the centre of the canyon (the x–z plane at $y/S = 0$) and on a horizontal plane located at the mid-height of the downwind building (the $x - y$ plane at $z/W \approx 0.5H_\text{d}$) in Sects. 5.1 and 5.2, respectively. We consider three different building-height ratios ($H_\text{d}/H_\text{u} \approx 0.08$, 0.27, and 0.69) for wide and narrow street canyons ($S/W \approx 2.5$ and $S/W \approx 1$, respectively). For the x–z plane, we compare the numerical results of the three CFD methods with each other and against published experimental data (Addepalli and Pardyjak 2015). For the horizontal plane, numerical results are only contrasted to each other for $H_\text{d}/H_\text{u} \approx 0.27$ due to the lack of experimental data. Finally, in Sect. 5.3 we analyze features of the velocity-field flow topology with both quantitative and qualitative metrics, and compare with experimental data.

To identify features of the flow topology from different datasets in a consistent manner, an identical streamline density represents the flow patterns, and features of the flow topology are extracted visually using the observed patterns. As numerical techniques for flow-topology

extraction (e.g., Helman and Hesselink 1991; Weinkauf et al. 2011) resulted in the detection of additional non-existent flow features, they are not employed here.

5.1 In-Canyon Along-Wind Centreplane ($x - z$ plane)

5.1.1 Canyon Configurations: $H_d/H_u \approx 0.08$, $S/W \approx 2.5$ *and 1*

Contours of the mean vertical velocity ($\overline{w}$) and streamline patterns computed from the three different CFD methods are shown with wind-tunnel PIV data in Figs. 4 and 5 for wide and narrow street canyons ($S/W \approx 2.5$ and $S/W \approx 1$), respectively, at the in-canyon along-wind centreplane. The experimental data for the wide street canyon (Fig. 4d) have the clear signature of a wake-dominated flow regime (Hussain and Lee 1980), where flow structures are strongly influenced by the upwind building. The presence of a saddle point (flow topological feature II in Fig. 4d) corresponding to an equilibrium point between the vertical flow from above the street canyon and horizontal flow around the upwind building, is a unique flow feature in this configuration (see Sect. 5.2 for the examination of horizontal flow patterns).

A counter-rotating vortex pair is observed in the canyon. A primary clockwise vortex forms above the saddle point in the upper left-hand corner of the street canyon (flow topological

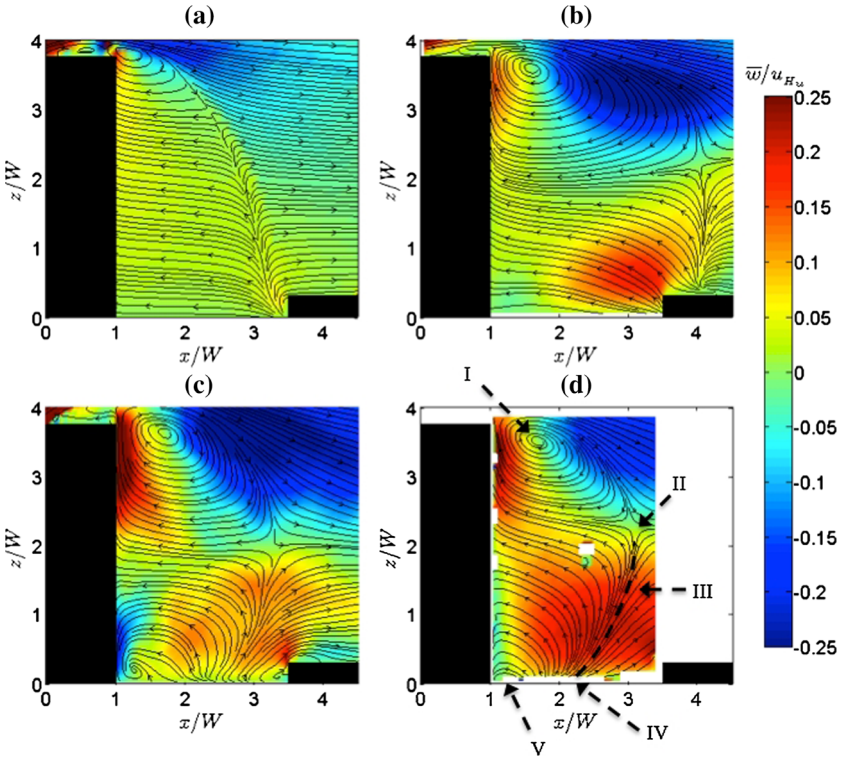

Fig. 4 Contours of the normalized mean vertical velocity at the in-canyon along-wind centreplane for a step-down street canyon for $H_d/H_u \approx 0.08$ and $S/W \approx 2.5$ (wide street canyon) as computed from the results of three CFD methods **a** QUIC-URB, **b** RANS, **c** LES, and from **d** experimental PIV data—Flow topological features I: Primary vortex core, II: Saddle point, III: Cavity-dividing streamline, IV: In-canyon separation point, V: Secondary vortex core

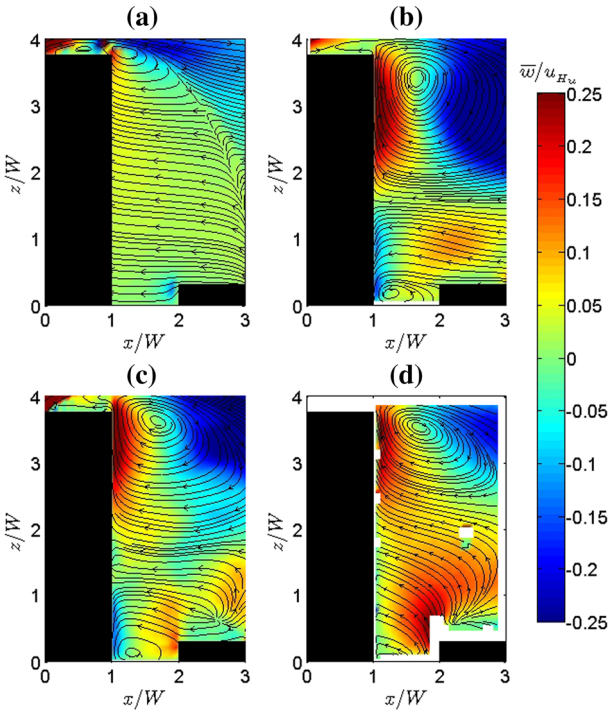

Fig. 5 Contours of normalized mean vertical velocity at the in-canyon along-wind centreplane for a step-down street canyon for $H_d/H_u \approx 0.08$, $S/W \approx 1$ (narrow street canyon) as computed from the results of three CFD methods **a** QUIC-URB, **b** RANS, **c** LES, and from **d** experimental PIV data

feature I in Fig. 4d) and a counter-clockwise secondary vortex forms below the saddle point in the lower left-hand corner of the street canyon (flow topological feature V in Fig. 4d). The secondary vortex is poorly resolved by the experimental data as a result of laser beam reflection and image acquisition errors near the building corners (Addepalli and Pardyjak 2015). The existence of an in-canyon separation streamline (described as a ground-originating shear layer by Addepalli and Pardyjak 2015) or a cavity-dividing streamline (flow topological feature III in Fig. 4d), is another prominent feature observed in the experimental data. The cavity-dividing streamline originates on the ground at the in-canyon separation point (flow topological feature IV in Fig. 4d), resulting from the convergence of the lateral flow downstream of the upwind building, leading to upwards flow towards the primary vortex and saddle point.

In comparing the numerical results with the experimental data, the QUIC-URB model significantly underpredicts the vertical flow in the lower half of the street canyon. In the upper half of the canyon, downwards vertical advection into the canyon from both the sides and the top of the upwind building is well simulated. The saddle point, in-canyon separation point and cavity-dividing streamline are roughly captured, but with the saddle point and cavity-dividing streamlines located much closer to the upwind and downwind buildings, respectively. The strength of the recirculation zone is much lower than indicated by the experimental data with a small primary vortex attached to the top corner of the upwind building. The secondary vortex is not observed in the QUIC-URB results.

RANS predicts the formation and location of the primary vortex better than QUIC-URB, but still fails to predict the counter-rotating vortex pair (Fig. 4b). As with QUIC-URB, RANS

results show the locations of saddle and in-canyon separation points inaccurately, with the separation point located on the rooftop of the downwind building. The strength of the vertical flow in the lower half of the canyon is greater than QUIC-URB, but still weaker than that for the experimental data. RANS also overestimates the wake of the upwind building by stretching the recirculation zone throughout the canyon, which moves the in-canyon separation point to the rooftop of the downwind building.

The LES results indicate that the counter-rotating vortex pair is correctly captured, with a secondary vortex located in the lower left-hand corner of the street canyon (Fig. 4c). The formation of the saddle point, the in-canyon separation point, and the curvature of the cavity-dividing streamlines are also in agreement with the experimental data. The LES model predicts the in-canyon separation point at the mid-width of the canyon. Note that even with LES, the strength of the vertical motion is still underestimated in the lower half of the street canyon.

Figure 5 shows that as the along-wind width of the street canyon decreases, the flow changes from a wake-dominated regime to a deep canyon skimming flow regime (Hussain and Lee 1980), where the downwind building has a much stronger impact on the upwind building's wake flow. As in the wide canyon case, there is a counter-rotating vortex pair, but the in-canyon separation point and dividing streamline rise to the rooftop of the downwind building (Fig. 5d). The secondary recirculation zone in the lower left-hand corner of the street canyon is not fully resolved due to PIV resolution issues (Addepalli and Pardyjak 2015).

In this narrow street-canyon case, QUIC-URB does not capture the substantial changes in flow regime, and erroneously predicts the flow equilibrium zone in the upper half of the canyon (Fig. 5a). The RANS model overestimates the strength of downwards advection in the upper half of the canyon and underestimates the flow updraft around the downwind building (Fig. 5b). Both RANS and LES models predict the counter-rotating vortex pair in the lower left-hand corner of the canyon (Fig. 5b, c), while RANS and QUIC-URB models fail to predict the in-canyon separation point and dividing streamline on the downwind building rooftop. In the LES results, the cavity-dividing streamline is slightly shifted downstream on the rooftop of the downwind building with respect to the experimental data (Fig. 5c). Here again, LES underpredicts the updrafts near and above the downwind building. All three methods erroneously predict disconnected flow regions in the upper and lower half of the canyon, while the experimental data indicate updrafts from the lower half of the canyon to the upper half.

Figure 6 shows the observed and simulated mean vertical velocity profiles along the centre of wide and narrow street canyons. In the lower half of the wide street canyon ($z/W < 2.0$), QUIC-URB predicts no updraft, while RANS and LES models underestimate it by ≈50% (Fig. 6a). As the width of the street canyon decreases, the strength of the vertical flow motions decrease significantly, and downwards advection into the vicinity of the canyon vanishes (Fig. 6b). In the lower half of the canyon ($0 < z/W < 2$), QUIC-URB again produces no updraft, while RANS and LES models significantly underestimate it by ≈65%. High above the canyon ($z/W > 3$), QUIC-URB produces significant downdrafts, while both RANS and LES models correctly predict the strength of the updrafts (Fig. 6b).

5.1.2 Canyon Configurations: $H_d/H_u \approx 0.27$, $S/W \approx 2.5$ *and 1*

Increasing the height of the downwind building from $H_d \approx 0.08H_u$ to $H_d \approx 0.27H_u$ does not significantly alter the dynamics of the mean flow in the street canyon (compare Figs. 4d and 7d). The main differences observed in the experimental data include the intensification of

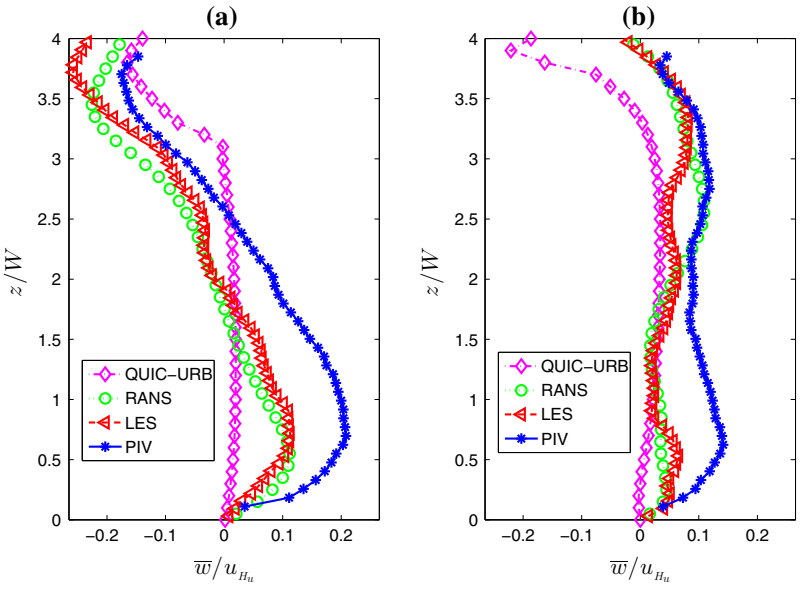

Fig. 6 Normalized mean vertical velocity profiles in the middle of the canyon for the step-down street canyon for $H_d/H_u \approx 0.08$, **a** $S/W \approx 2.5$ (wide street canyon), **b** $S/W \approx 1$ (narrow street canyon)

updrafts and a vertical shift upwards of the saddle point, which indicate increased interaction between the downwind and upwind buildings.

The results from the QUIC-URB simulation are similar to those in Sect. 5.1.1. The primary departure is a shift in the location of the separation streamline, which moves from the bottom corner of the downwind building to the upper corner (Fig. 7a). The RANS results are also similar to those described in Sect. 5.1.1, including a lack of any secondary recirculation. The primary difference is that the location of the saddle point is shifted slightly upwards (Fig. 7b). Increasing the downwind building height to $0.27H_u$ has a minimal impact on the performance of the LES model. As with the $0.08H_u$ case, LES captures the primary topological features, but underestimates the vertical updraft strength in the canyon. As a result, LES places the saddle point at a lower height in the canyon compared with the PIV data (Fig. 7c). Additionally, the secondary vortex in the lower right-hand corner of the street canyon is exaggerated in extent (Fig. 7c).

As shown in Fig. 8d, when the width of the street canyon is decreased, the experimental data have two noticeable changes from the $H_d/H_u \approx 0.08$ narrow street-canyon case. The first is a decrease in the apparent extent of the updraft region in the lower right-hand corner of the canyon, and the second is an associated movement of the source above the downwind building in the positive x direction (Fig. 8d). Again, QUIC-URB fails to simulate changes in the flow topology associated with an increase in the downwind building height, by erroneously predicting a street-canyon vortex at the height of the downwind building (Fig. 8a), due to the street-canyon-flow algorithm having been designed mostly based on data collected within buildings of equal height (Singh et al. 2008). The QUIC-URB and LES models both approximately capture the strength of the updrafts, while the RANS model strongly underestimates it. All numerical simulations overestimate the experimentally observed downdraft flow motions close to the upwind building at $1 < x/W < 1.2$ and $0 < z/W < 1.2$. This

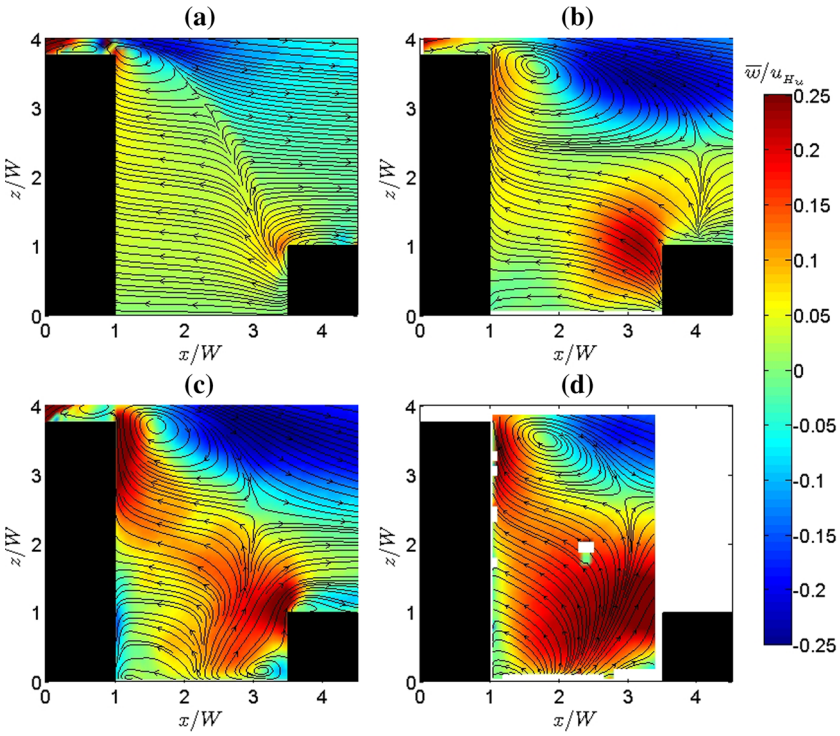

Fig. 7 Contours of normalized mean vertical velocity at the in-canyon along-wind centreplane for a step-down street canyon for $H_d/H_u \approx 0.27$, $S/W \approx 2.5$ (wide street canyon) as computed from three CFD methods **a** QUIC-URB, **b** RANS, **c** LES, and from **d** experimental PIV data

overly strong downdraft is associated with the street-canyon parametrization in QUIC-URB (designed for buildings of equal height) and the underestimation of the lower canopy updraft by the RANS and LES models. The mean vertical velocity profiles in the middle of the along-wind centreplane are similar to those observed in Sect. 5.1.1.

5.1.3 Canyon Configurations: $H_d/H_u \approx 0.69$, $S/W \approx 2.5$ *and 1*

Contours of mean vertical velocity ($\overline{w}$) and streamlines computed from different CFD methods and PIV data are shown in Figs. 9 and 10 for wide and narrow street canyons ($S/W \approx 2.5$ and $S/W \approx 1$), respectively, at the along-wind centreplane. The experimental data for the wide street canyon (Fig. 9d) still indicate a wake-dominated flow regime, but the effect of the downwind building on the street-canyon cavity is more significant than the shorter downwind building cases. This impact manifests in the strengthening of the updrafts, the decrease in the absolute distance between saddle point and primary vortex, and a shift of the in-canyon separation point towards the downwind building. Note that the flow-regime transition from wake dominated to deep wake interference occurs at greater building-height ratios ($H_d/H_u > 0.88$, Addepalli and Pardyjak 2015).

None of the computational methods successfully captures all features of the flow topology for this configuration, though the QUIC-URB model still predicts a vortex attached to the top corner of the upwind building. While QUIC-URB is the only model that correctly captures the

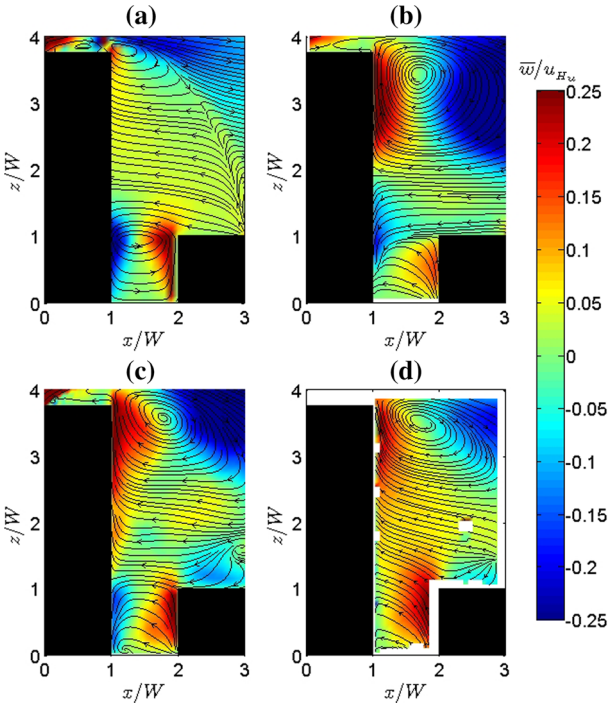

Fig. 8 Contours of normalized mean vertical velocity at the in-canyon along-wind centreplane for a step-down street canyon for $H_d/H_u \approx 0.27$, $S/W \approx 1$ (narrow street canyon) as computed from three CFD methods **a** QUIC-URB, **b** RANS, **c** LES, and from **d** experimental PIV data

saddle point in the upper half of the canyon, this model misses the vertical flow in the lower half of the canyon (Fig. 9a). The RANS and LES models both improve the representation of updrafts compared with QUIC-URB (Fig. 9b, c), with LES arguably better, but neither model reproduces the in-canyon separation point observed in the experiments. LES is the only method that captures the double counter-rotating secondary vortices at the bottom corners of the buildings (Fig. 9c). The LES and RANS models both overpredict the impact of the downwind building on the canyon cavity and the transition to the deep-wake interference regime at a lower building-height ratio compared with the experimental data (see Addepalli and Pardyjak 2015).

As the width of the street canyon decreases for this building configuration (Fig. 10), the taller downwind building induces stronger updrafts in the canyon compared with the $H_d/H_u \approx 0.27$ case. The updrafts are intensified up to the height of the downwind building within the entire canyon. The deep canyon skimming-flow regime is dominant, and a static vortex manifests itself at the top of the canyon (Fig. 10d). For this case, the QUIC-URB model significantly underestimates the updrafts in the canyon and produces an erroneous vortex at the height of the downwind building similar to the $H_d/H_u \approx 0.27$ case, while also predicting an unexpected saddle point at the top of the canyon (Fig. 10a). The RANS model results indicate strong downwards advection from the rooftop cavity of the downwind building towards the upwind building for $2 < z/W < 2.5$, leading to the spurious generation of a secondary vortex in the middle of the canyon (Fig. 10b). The LES model also results in a downwards advection at $z/W \approx 2.5$ into the canyon not observed in the experiments,

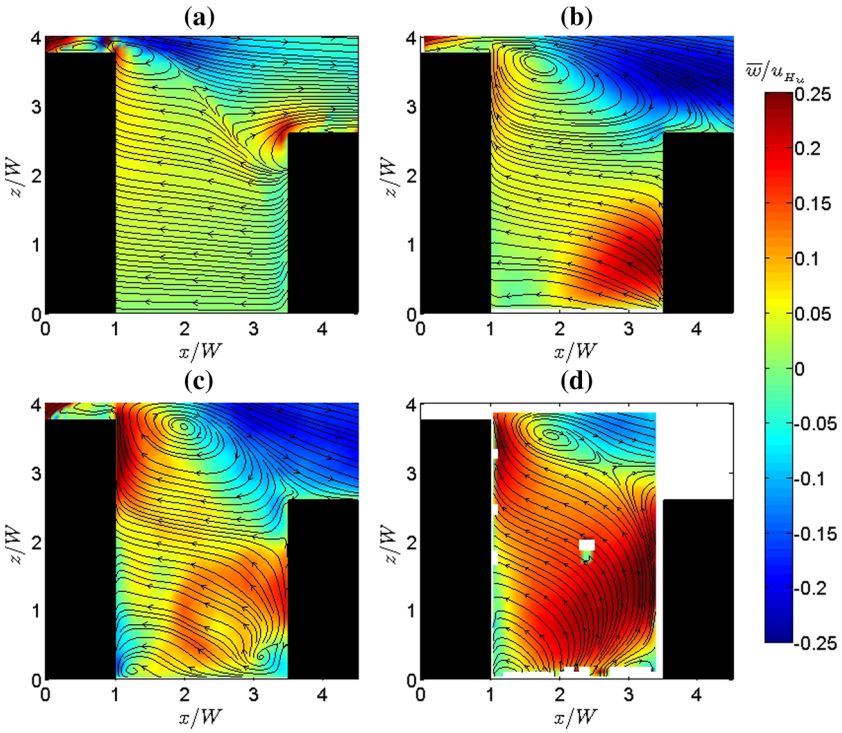

Fig. 9 Contours of normalized mean vertical velocity for a step-down street canyon for $H_d/H_u \approx 0.69$, $S/W \approx 2.5$ (wide street canyon) as computed from three CFD methods **a** QUIC-URB, **b** RANS, **c** LES, and from **d** experimental PIV data

but at a lower magnitude over a much smaller region (Fig. 10c). As a result, the secondary vortex observed in the RANS flow field does not appear in the LES results. All three models predict the primary vortex, with QUIC-URB significantly underestimating the strength and the development of the recirculation zone at the top of the canyon.

The mean vertical velocity profiles in the middle of the along-wind centreplane are similar to those observed in Sect. 5.1.1.

5.2 Canyon Horizontal Plane

The previous sections illustrate the mean velocity-field dynamics of the three methods in a vertical cross-section. Here, a horizontal plane located at the mid-height of the downwind building ($z/W \approx 0.5H_d$) is used to explore the wake-flow propagation around the buildings. Since PIV data were not collected in the horizontal plane, the numerical results are only inter-compared, and only for wide and narrow street canyons ($S/W \approx 2.5$ and $S/W \approx 1$) with $H_d/H_u \approx 0.27$ (Figs. 11 and 12). For the wide street canyon, the LES results show that the lateral flow, i.e., horizontal flow entering the canyon from the sides, and the canyon-cavity flow both strongly contribute to the formation of a counter-rotating vortex pair, as well as a flow equilibrium zone at the mid-width of the canyon ($y/W \approx 0$, $x/W \approx 2.2$) (Fig. 11c). The interaction between the lateral and canyon-cavity flows leads to a flow equilibrium in the middle of the canyon. As a result, one observes the separation of flow from the ground,

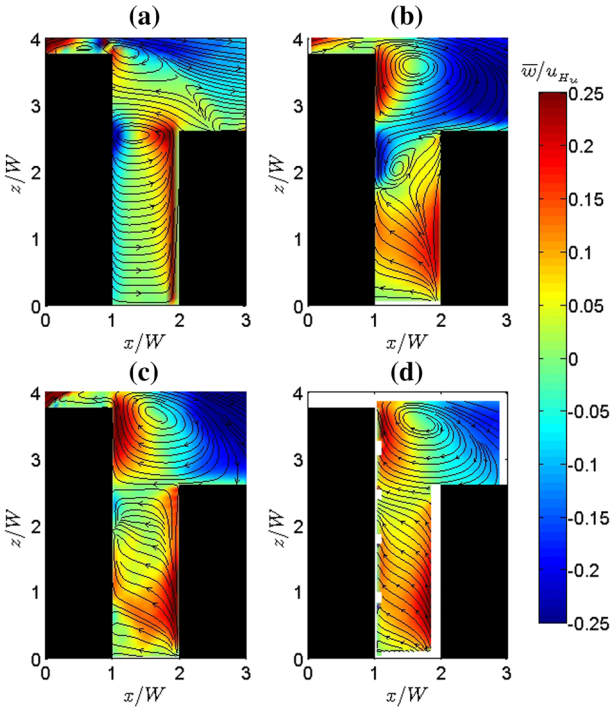

Fig. 10 Contours of normalized mean vertical velocity for a step-down street canyon for $H_d/H_u \approx 0.69$, $S/W \approx 1$ (narrow street canyon) as computed from three CFD methods **a** QUIC-URB, **b** RANS, **c** LES, and from **d** experimental PIV data

and the formation of a cavity-dividing streamline and a saddle point as illustrated by the vertical planes (Fig. 7c). Flow separates from the leading edge of the upwind building to form lateral recirculation zones, resulting in an increase in the width of the canyon-wake flow. In the wake of the downwind building, a counter-rotating vortex pair develops from the building trailing edge ($x/W \approx 4.5$) up to $x/W \approx 5.2$ with the vortex core located at $x/W \approx 4.75$. Comparing QUIC-URB with LES model results, the vertical velocity is significantly underestimated, except for a small region at the upwind cavity of the upwind building (Fig. 11a). The wake of the upwind building dominates the entire street canyon with a strong counter-rotating vortex pair stretched between the two buildings. Moreover, the depth of the sidewall separation is much smaller and the sidewall counter-rotating vortex pair is not resolved. Note that, in previous QUIC-URB versions without the building sidewall recirculation algorithm, no sidewall recirculation was predicted.

In the wake of the upwind building, RANS results show a counter-rotating vortex pair that is also larger than that for the LES results. The RANS model exaggerates the coherence of the flow structures even more than QUIC-URB; the entire street canyon is dominated by a large counter-rotating vortex pair with the vortex core located farther downstream of the upwind building ($x/W \approx 1.75$) compared with QUIC-URB ($x/W \approx 1.5$) and LES ($x/W \approx 1.25$) (Fig. 11b). Similarly, the RANS model downwind-building wake develops over a much larger zone compared with QUIC-URB and LES. The vertical velocity and the sidewall counter-rotating vortex pair are also larger than QUIC-URB, but still smaller than LES model results. Note that none of the models predicts separation from the downwind

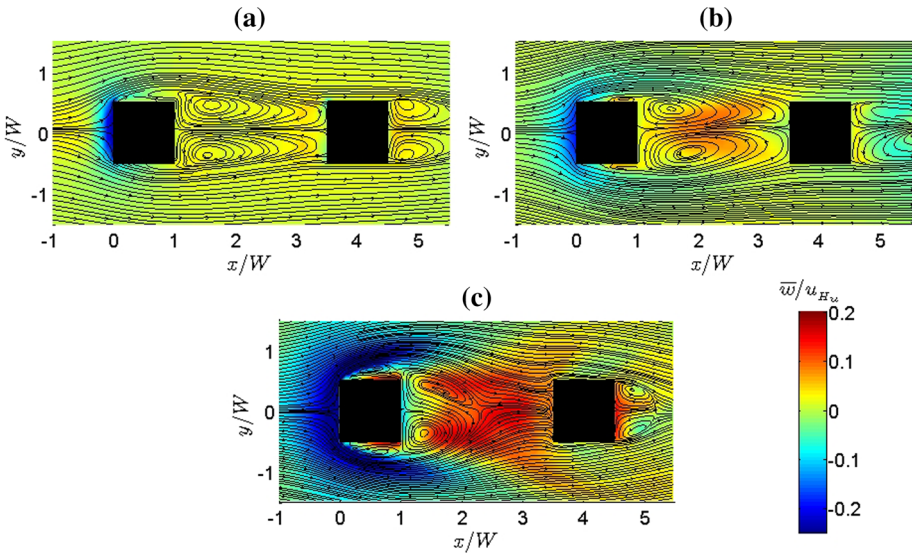

Fig. 11 Wake-field distribution in a wide step-down street canyon for $H_d/H_u \approx 0.27$, $S/W = 2.5$ at the mid-height of the downwind building ($z/H_d \approx 0.5$) as computed from three CFD methods **a** QUIC-URB, **b** RANS, and **c** LES

building sidewalls. As a result, the width of the downwind building wake is narrower in extent than the canyon-recirculation region, indicating the correct logic of the QUIC-URB model in not applying the sidewall algorithm to the downwind building.

As the width of the street canyon decreases, LES no longer predicts the in-canyon saddle point, and the counter-rotating vortex pair covers the entire canyon cavity (Fig. 12c). The lack of interaction between vertical flow downwards into the canyon and the lateral flow entering the canyon results in a deep canyon skimming-flow regime as discussed in Sect. 5.1.2. Other than the dominance of the recirculation zone in the street-canyon cavity, the wake structures are similar to the case of the wide street canyon. The RANS results show a counter-rotating vortex pair in the canyon cavity similar to LES, but the wake of the downwind building is much larger, stretching to $x/W \approx 5.3$ with a much stronger counter-rotating vortex core located at $x/W \approx 4$ compared with $x/W \approx 3.5$ for LES (Fig. 12b). In examining the RANS model results for both cases, one observes that a coherent recirculation zone in the canyon cavity dominates the entire canyon (for the cases considered), and is bounded by the downwind building.

Overall, the results in the horizontal plane validate the hypothesis of Addepalli and Pardyjak (2015) that the features and dynamics observed in the vertical plane are indicators of the interaction between lateral and vertical flow motions.

5.3 Flow Topological Features

5.3.1 Dynamics Tracking

It is instructive to determine how each CFD method tracks changes in topological features in the flow as a function of street-canyon geometry in comparison with the PIV data (Fig. 13). Only the wide street-canyon case is presented, as the narrow street canyons only have a

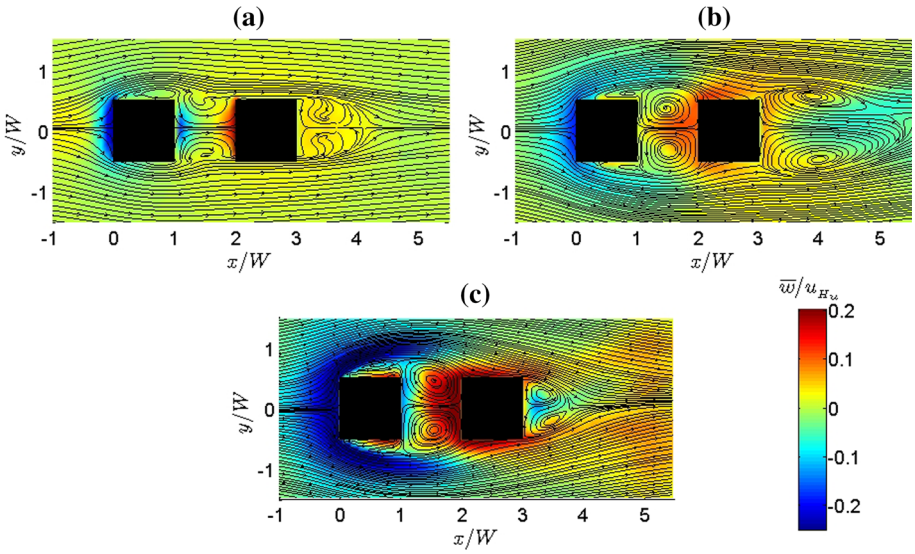

Fig. 12 Wake-field distribution in a narrow step-down street canyon for $H_d/H_u \approx 0.27$, $S/W = 1$ at the mid-height of the downwind building ($z/H_d \approx 0.5$) as computed from three CFD methods **a** QUIC-URB, **b** RANS, and **c** LES

single strong topological feature (the vortex just below and downwind of the top of the upwind building), which is a very weak function of H_d. The source that appears above the downwind building only appears with small H_d and is not tracked here. The experimental data indicate that, as the height of the downwind building increases (H_d/H_u increases), the saddle point elevates towards the top of the street canyon and shifts closer to the upwind building. The QUIC-URB and RANS methods significantly underestimate and overestimate the downstream distance to the saddle point by ≈0.5 and ≈1.5 W, respectively (Fig. 13a). The erroneous prediction of the streamwise location of the saddle point by QUIC and RANS models is directly associated with the interaction of the horizontal recirculation zones (Sect. 5.2) and the flow equilibrium (Sect. 5.1). While the LES model appears to correctly predict the streamwise location of the saddle point, it underpredicts the saddle-point elevation by ≈1 W, likely related to the weaker updrafts discussed in Sect. 5.1. From the eight test cases simulated with QUIC-URB and RANS, QUIC-URB qualitatively predicts the saddle point in all test cases, while the RANS model fails to capture the feature in three cases (i.e., $H_d/H_u \approx 0.53$, 0.61, and 0.69). Even LES could not predict the feature for $H_d/H_u \approx 0.69$ from the five examined test cases (Fig. 13a).

For the primary vortex, the experimental data suggest that the vertical position is independent of the building-height ratio. As the height of the downwind building increases, the vortex moves horizontally towards the downwind building (Fig. 13b), which is likely related to the enhanced wake interaction between the upwind and downwind buildings for increased building-height ratios. From the studied test cases, all three methods qualitatively capture the primary vortex (Fig. 13b), and successfully predict the vertical location of the vortex core. In the streamwise direction, the QUIC-URB model underestimates the location of the vortex core by ≈0.5 W. As the building-height ratio increases, the primary vortex as modelled by QUIC-URB remains stationary.

As the downwind building height increases, the origin of the in-canyon separation point shifts towards the downwind building due to the intensified interaction between the lateral

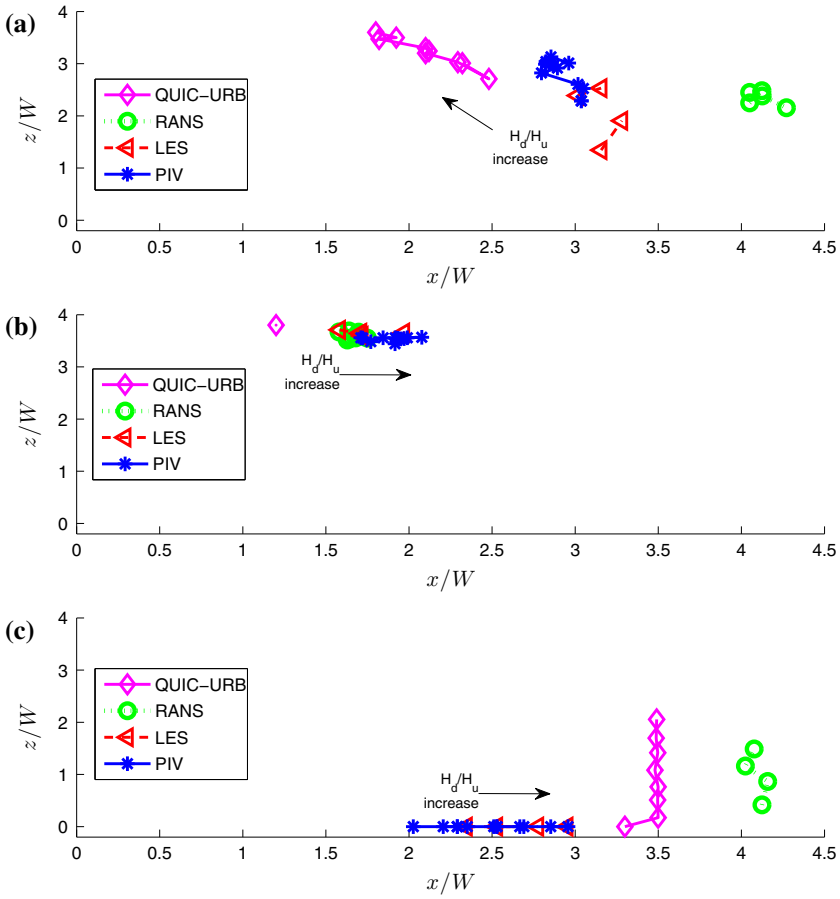

Fig. 13 Spatial variation of three flow topological features (**a** saddle point, **b** vortex core, and **c** in-canyon separation point) in wide step-down street canyons with downwind-to-upwind building-height ratios covering the range: $0 \leqslant H_d/H_u \leqslant 0.69$

flow and the street-canyon cavity (Fig. 13c). LES is the only method that correctly captures the in-canyon separation point and accurately predicts the horizontal inclination of this feature, while the QUIC-URB and RANS methods fail in the modelling of its spatial variation. Both result in a static streamwise location for the in-canyon separation point on the leading edge of the downwind building ($x/W \approx 3.5$) and the rooftop of the downwind building ($x/W \approx 4.1$), respectively. From the eight test cases simulated with QUIC-URB and RANS models, the QUIC-URB method qualitatively predicted the in-canyon separation point on the ground (i.e., $z/W \approx 0$) only for $H_d/H_u \approx 0.08$, while the RANS method failed to capture the feature on the ground for all cases (Fig. 13c). Even LES does not predict the feature for $H_d/H_u \approx 0.69$ (Fig. 13c).

5.3.2 Accuracy and Capability

Here, we quantify the ability of the three CFD methods to predict the locations of the various flow topological features and the entire velocity field in the in-canyon along-wind centreplane

of step-down street canyons using the mean relative error ($\overline{\epsilon}_R$), the bounded normalized mean-square error (*BNMSE*) (Warner et al. 2006) and the coefficient of determination (R^2) defined as

$$\overline{\epsilon}_R = \frac{1}{T}\sum_{h=1}^{T}\sqrt{\left(\frac{|x_h^{num} - x_h^{exp}|}{x_h^{exp}}\right)^2 + \left(\frac{|z_h^{num} - z_h^{exp}|}{z_h^{exp}}\right)^2} \times 100, \tag{7a}$$

$$BNMSE = \frac{\sum_{a=1}^{E}(c_a^{num} - c_a^{exp})^2}{\sum_{a=1}^{E}(c_a^{num} + c_a^{exp})^2}, \tag{7b}$$

$$R^2 = 1 - \frac{\sum_{a=1}^{E}(c_a^{\mathrm{num}} - c_a^{\mathrm{exp}})^2}{\sum_{a=1}^{E}(c_a^{\mathrm{exp}} - \overline{c})^2}, \tag{7c}$$

respectively. In Eq. 7a, h is the index for the test cases and T is the total number of test cases simulated by each method (i.e., $T = 8$ for QUIC-URB and RANS and $T = 5$ for LES), $\overline{\epsilon}_R$ is the mean relative error in the prediction of each flow topological feature's location with different CFD methods with respect to the experimental data, x_i^{num} and z_i^{num} are the simulated x and z locations of the flow topological features for each test case ($S/W \approx 2.5, 0 \leqslant H_{\mathrm{d}}/H_{\mathrm{u}} \leqslant 1$), whereas x_i^{exp} and z_i^{exp} are the experimental x and z locations. In Eq. 7b, a indexes all simulated points in the entire street canyon, i.e., $1 \leqslant x/W \leqslant 3.5, 0 \leqslant z/W \leqslant 4$), and c_a^{num} and c_a^{exp} are the simulated and experimental streamwise and vertical velocity components, respectively, with $\overline{c}$ the mean velocity component.

LES performs well for all features, with a relative error of ≈21% for both the saddle and in-canyon separation points, and 6% for the vortex core (Fig. 14). QUIC-URB and RANS models locate the saddle point with errors of ≈30 and ≈42%, respectively. The RANS model is superior at locating the vortex (≈10%), while QUIC-URB's inability to track the core's movement results in a poor overall performance (≈38% error). Neither the QUIC-URB nor RANS model is capable of simulating the in-canyon separation point correctly, leading to a relative error of ≈115 and 130%, respectively. For narrow step-down street canyons, all methods predict the location of the major vortex core reasonably well with errors of about 21, 9, and 6% for the QUIC-URB, RANS, and LES methods, respectively.

QUIC-URB outperforms the RANS model in simulating the streamwise velocity component in all test cases of wide street canyons as evident in the smaller $BNMSE$ and higher R^2 values (Fig. 15a, c). However, RANS is significantly better than QUIC-URB for the vertical velocity component with smaller $BNMSE$ and higher R^2 values (Fig. 15b, d). In all test cases, LES has the best agreement with the measurements, having the lowest $BNSME$ and highest R^2 values (Fig. 15a–d). QUIC-URB performance deteriorates almost monotonically with higher H_d for both streamwise and vertical velocity components (Fig. 15a, b) due to the inadequacy of its flow parametrization algorithms. Both RANS and LES results indicate non-monotonic degradation in vertical velocity with the highest $BNSME$ and lowest R^2 values at $H_{\mathrm{d}}/H_{\mathrm{u}} \approx 0.69$ (Fig. 15b, d).

Tables 5 and 6 qualitatively summarize the capabilities of the CFD methods to predict major flow topological features in wide and narrow step-down street canyons. For wide street

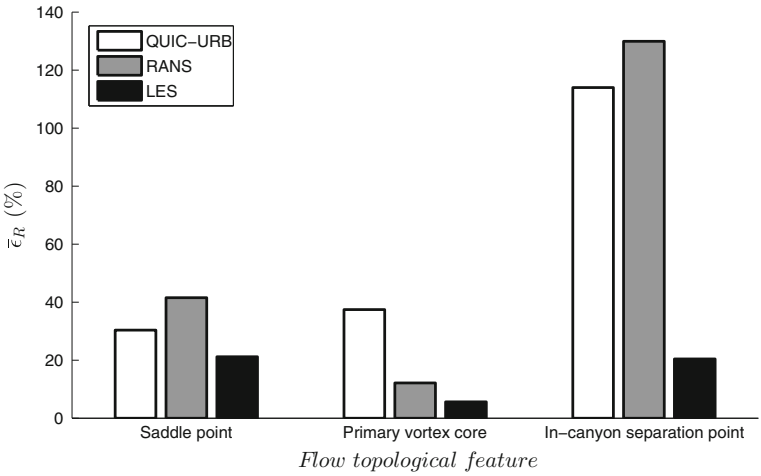

Fig. 14 The mean relative error of flow topological features in wide step-down street canyons using different CFD methods

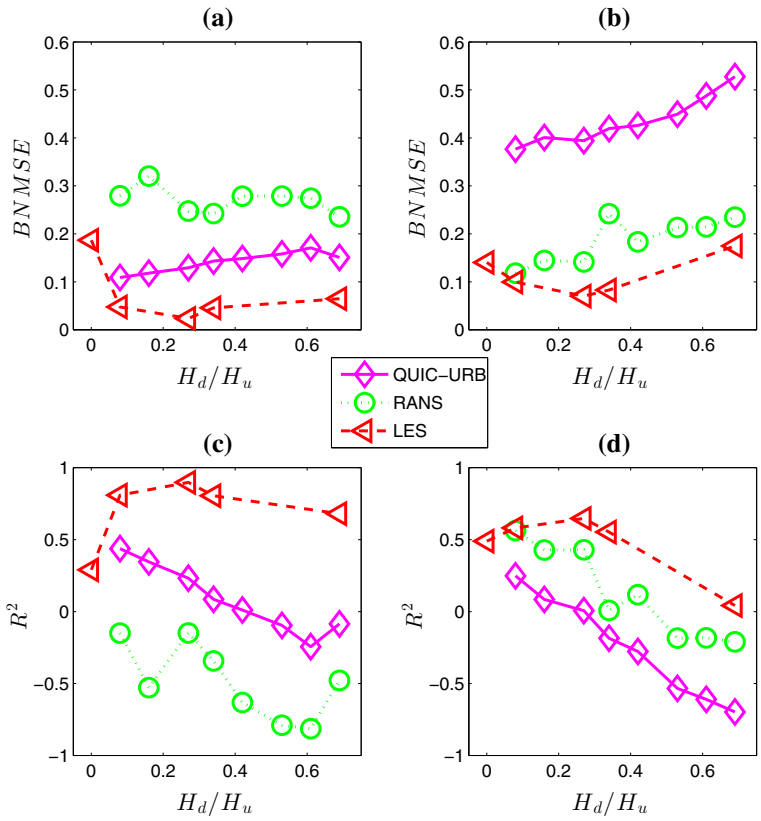

Fig. 15 Velocity-field error metrics for wide step-down street canyons ($1 \leqslant x/W \leqslant 3.5, 0 \leqslant z/W \leqslant 4$) for the different CFD methods: **a** *BNMSE* for streamwise velocity component, **b** *BNMSE* for vertical velocity component, **c** R^2 for streamwise velocity component, and **d** R^2 for vertical velocity component

Table 5 Qualitative comparison of the capability of different CFD methods in capturing the flow topological features in wide step-down street canyons

Method	Saddle point	Primary vortex	In-canyon separation point	Secondary vortex
QUIC-URB	Always	Always	Seldom	Never
RANS	Often	Always	Never	Never
LES	Often	Always	Often	Always

Table 6 Qualitative comparison of the capability of different CFD methods in capturing the flow topological features in narrow step-down street canyons

Method	Primary vortex	Secondary vortex
QUIC-URB	Always	Never
RANS	Always	Always
LES	Always	Always

canyons, QUIC-URB is the only method that includes the saddle point for all of the tested downwind building heights. However, both the LES and RANS methods simulate the feature for more than half of the test cases and LES does a superior job of correctly positioning the saddle point (Fig. 14). The primary vortex is a relatively well-predicted topological feature for all of the methods and for different street-canyon configurations. In contrast, the in-canyon separation point is collectively by far the most difficult feature to predict. Neither the QUIC-URB nor RANS model is successful in simulating it on the ground; QUIC-URB only predicts the feature for a few of the street-canyon configurations, while RANS never produces an in-canyon separation point. LES is the only method that successfully captures the location of the in-canyon separation point for many of the cases. Even with LES, there are still a few instances where the method fails to predict this feature. The secondary vortices are also difficult for RANS and QUIC-URB to simulate, and LES is again the only method that successfully produces this feature in the proximity of the bottom corners of the upwind and downwind buildings. For narrow step-down street canyons, qualitative predictions of flow topological features are generally better with a few caveats (Table 6). While all methods are capable of predicting the primary vortex, both RANS and LES models successfully predict the secondary vortex, while QUIC-URB is unable to resolve the feature. A second issue is that both QUIC-URB and RANS methods sometimes produce an extra street-canyon vortex between the two buildings at the height of the downwind building as discussed in Sect. 5.1.3.

6 Conclusions

We evaluated the ability of three different CFD methods to predict important flow structures and topological features in step-down street canyons (i.e., a tall building followed by a short building), by comparing methods with high-spatial-resolution two-dimensional wind-tunnel data. We used a novel and comprehensive evaluation process to focus on the dynamics of flow topological features that form as a result of different geometric configurations. We highlight the strengths and deficiencies of CFD methods with different levels of flow-physics modelling in tracking the spatial variability of the dominant flow topological features in street canyons

with uneven building heights and explain requirements for further improvements of the CFD methods in urban-flow studies.

The methods we evaluate include a fast-response empirically-based flow model (QUIC-URB), a mean Navier–Stokes solver (RANS), and a fully three-dimensional unsteady Navier–Stokes solver (LES). We consider street-canyon widths ($S/W \approx$1–2.5) and downwind-to-upwind building-height ratios (0–0.69), including very small to tall downwind buildings.

Canyon along-wind centreplane ($x - z$ plane) numerical results suggest that QUIC-URB does not properly predict flow-regime transitions as the canyon configuration changes. A consistent problem is the substantial underestimation of vertical flow motions deep in the canyon. While the RANS method performed better than the QUIC-URB method, it still partially fails to predict flow-regime characteristics, particularly in the case of wide street canyons, where the in-canyon separation point fails to be predicted. Moreover, the interaction of the lateral flow and the street-canyon cavity flow is dominated by an exaggerated recirculation zone at the top of the upwind building. The LES method yields the most reasonable results with the correct prediction of the flow regime characteristics in most of the studied canyon configurations, capturing the in-canyon separation point and secondary recirculation zones in wide street canyons. A horizontal plane inter-comparison of the three methods shows good agreement between the models in the prediction of building sidewall separation zones and their growth from the upwind building leading edge. Although all methods agree on the sidewall flow features, this is not the case for flow interactions between the recirculation and flow equilibrium zones in the canyon. The RANS model strongly overestimates the coherence of the structures compared with QUIC-URB and LES. In particular, RANS exaggerates the development of the counter-rotating vortex pairs in the street-canyon cavity and behind the downwind building.

In checking the resolution sensitivity for each method, we found a required resolution for capturing the recirculation zones for both QUIC-URB and RANS methods of 3.2, and 2 m for LES. LES is superior both qualitatively and quantitatively in capturing the evolution of the complex flow topological features with changing street-canyon geometry, while QUIC-URB and RANS both struggle with some features. However, even LES fails to predict the in-canyon separation and saddle points at high downwind building heights, and underestimates the strength of updrafts in the canyon. The QUIC-URB method outperforms (underperforms) the RANS method for wide (narrow) street canyons. Some non-physical flow topological features were produced by both QUIC-URB and RANS for a number of canyon configurations. The accuracy of each CFD method in the prediction of different flow topological features deteriorates for street canyons with larger along-wind street-canyon widths. In wide street canyons, QUIC-URB outperforms RANS in the prediction of the streamwise velocity component, while the RANS method better predicts the vertical velocity component. The QUIC-URB method becomes almost monotonically poorer for increasing downwind building heights. With both the RANS and LES methods, results for the vertical velocity component deteriorates non-monotonically with greater downwind building heights.

Not surprisingly, LES yields the most realistic predictions of the complex flow structures for the street-canyon cases considered. However, the computational cost of even a single test case is much higher than either the QUIC-URB or RANS methods, with over 20,000,000 and 1400 times more CPU hours required per simulation, respectively. In addition, the strong sensitivity of LES results to the inflow and the difficulties in generating the appropriate upstream profiles, are challenging aspects of this method. Thus, the general applicability of LES in practical engineering problems for urban-flow studies is significantly limited, so that improving low-cost reliable CFD methods is a necessity.

We highlight here the requirements for improvements in different CFD methods by quantifying the discrepancies in the prediction of dominant flow topological features in street canyons with uneven building heights. The QUIC-URB method needs to account for transitions in the flow regime, as well as for vertical flow in the lower half of the street canyons. The RANS method requires improvements in turbulence closure schemes and boundary conditions. The LES method fails to capture some of the flow topological features at high downwind building heights and underestimates vertical motions, indicating the need for further improvements in subgrid-scale turbulence models and surface and inflow boundary conditions.

Overall, for future improvements of CFD methods in urban-flow studies, it is essential to focus more on the capability to reproduce the dynamics of flow topological features with geometric changes in complex street canyons. High-spatial-resolution wind-tunnel data have a critical role in rigorous evaluation of the methods. Flow analysis around rotated and isolated buildings, step-up street canyons (i.e., a short building followed by a tall building) with various building widths, and realistic full-scale cities, are further critical steps needed to identify the parameter space over which different CFD methods are valid, and to characterize their reliability, thus increasing their adoption and usage in urban design and planning.

Acknowledgements This research was supported by National Science Foundation grants IDR CBET-PDM 1134580 and CBET 1512740. Additional funding was provided by the University of Utah Graduate School and the Global Change and Sustainability Center at the University of Utah. We would like to acknowledge current and previous Uintah infrastructure developers. Our LES results would not be possible without them. We also acknowledge high-performance computing support from Yellowstone (ark:/85065/d7wd3xhc) provided by NCAR's Computational and Information Systems Laboratory, sponsored by the National Science Foundation. This work also used the Extreme Science and Engineering Discovery Environment (XSEDE), which is supported by National Science Foundation grant number ACI-1053575.

References

Addepalli B, Pardyjak E (2015) A study of flow fields in step-down street canyons. Environ Fluid Mech 15:439–481

Alegrini J, Dorer V, Carmeliet J (2014) Buoyant flows in street canyons: validation of CFD simulations with wind tunnel measurements. Build Environ 72:63–74

Allwine KJ, Flaherty JE, Brown M, Coirier W, Hansen O, Huber A, Leach M, Patnaik G (2008) Urban dispersion program: evaluation of six building-resolved urban dispersion models. Technical report PNNL-17321, Pacific Northwest National Laboratory, Richland, WA

Apsley D, Castro I (1997) Flow and dispersion over hills: comparison between numerical predictions and experimental data. J Wind Eng Ind Aerodyn 67–68:375–386

Arnfield A (2003) Two decades of urban climate research: a review of turbulence exchanges of energy and water and the urban heat island. Int J Clim 23:1–26

Blocken B (2015) Computational fluid dynamics for urban physics: importance, scales, possibilities, limitations and ten tips and tricks towards accurate and reliable simulations. Build Environ 19:219–245

Blocken B, Persoon J (2009) Pedestrian wind comfort around a large football stadium in an urban environment: CFD simulation, validation and application of the new Dutch wind nuisance standard. J Wind Eng Ind Aerodyn 97(5–6):255–270

Blocken B, Stathopoulos T (2013) CFD simulation of pedestrian-level wind conditions around buildings: past achievements and prospects. J Wind Eng Ind Aerodyn 121:138–145

Britter R, Hanna S (2003) Flow and dispersion in urban areas. Annu Rev Fluid Mech 35:1817–1831

Britter R, Schatzmann M (2007) Background and justification document to support the model evaluation guidance and protocol of microscale meteorological models. COST Office, Brussels, pp 1–28

Brown M, Gowardhan AA, Nelson MA, Williams M, Pardyjak ER (2013) QUIC transport and dispersion modelling of two releases from the Joint Urban 2003 field experiment. Int J Environ Pollut 52(3–4):263–287

Chung D, Malone-Lee L (2010) Computational fluid dynamics for urban design. In: New frontiers - proceedings of the 15th international conference on computer-aided architectural design in Asia, CAADRIA 2010, Hong Kong, pp 357–366
Collier G (2006) The impact of urban area on weather. Q J R Meteorol Soc 132:1–25
Comte-Bellot G, Corrsin S (1966) The use of a contraction to improve the isotropy of grid-generated turbulence. J Fluid Mech 25(4):657–682
Fernando HJS, Lee SM, Anderson J, Princevac M, Pardyjak E, Grossman-Clarke S (2001) Urban fluid mechanics: air circulation and contaminant dispersion in cities. Environ Fluid Mech 1(1):107–164
Germain JDdS, McCorquodale J, Parker SG, Johnson CR (2000) Uintah: a massively parallel problem solving environment. In: 9th IEEE international symposium on high performance and distributed computing. IEEE, Piscataway, NJ, pp 33–41
Germano M, Piomelli U, Moin P, Cabot W (1991) A dynamic sub-grid scale eddy viscosity model. Phys Fluids A 3(7):1760–1765
Gousseau P, Blocken B, van Heijst G (2013) Quality assessment of large-eddy simulation of wind flow around a high-rise building: validation and solution verification. Comput Fluids 79:120–133
Gowardhan A, Brown M, Williams M, Pardyjak E (2006) Evaluation of the QUIC Urban Dispersion Model using the Salt Lake City URBAN 2000 Tracer Experiment Data-IOP 10. In: 6th AMS Symp Urban Env, Amer Meteor Soc, Atlanta, GA, LA-UR-05-9017, 13 pp
Gowardhan A, Brown M, Pardyjak E (2010) Evaluation of a fast response pressure solver for flow around isolated cube. Environ Fluid Mech 10:311–328
Gross G (1997) ASMUS-ein numerisches modell zur berechnung der stromung und der schadtstoffverteilung im bereich einzelner gebaude. ii: Schadstoffausbreitung und anwendung. Meteorol Zeitschrift 6:130–136
Guilkey J, Harman T, Banerjee B (2007) An Eulerian Lagrangian approach for simulating explosions of energetic devices. Comput Struct 85(11–14):660–674
Hang J, Sandberg M, Li Y (2009) Effect of urban morphology on wind condition in idealized city models. Atmos Environ 43:869–878
Hanna S, White J, Trolier J, Vernot R, Brown M, Gowardhan A, Kaplan H, Alexander Y, Moussafir J, Wang Y, Williamson C, Hannan J, Hendrick E (2011) Comparisons of JU2003 observations with four diagnostic urban wind flow and Lagrangian particle dispersion models. Atmos Environ 45(24):4073–4081
Hayati AN, Stoll R, Harman T, Pardyjak E (2014) Large-eddy simulation of street canyons and urban microclimate using Uintah: MPMICE. Abstract A43A-3243 presented at 2014, Fall Meeting, AGU, San Francisco, CA, USA, 15–19 December
Hayati AN, Stoll R, Harman T, Pardyjak E (2016) Large-eddy simulation of the oklahoma city joint urban 2003 experiment using Uintah: MPMICE. In: 22nd Symposium on boundary layers and turbulence, American Meteor Society, Salt Lake City, UT, USA
Helman JL, Hesselink L (1991) Visualizing vector field topology in fluid flows. IEEE Comput Graphics Appl 11(3):36–46
Hertwig D, Efthimiou G, Bartzis J, Leitl B (2012) CFD-RANS model validation of turbulent flow in a semi-idealized urban canopy. J Wind Eng Ind Aerodyn 111:61–72
Hosker RP (1984) Flow and diffusion near obstacles. In: Randerson D (ed) Atmospheric science and power production, US Department of Energy DOE/TIC-27601 (DE 84005177), Springfield, Virginia, USA, chap 7, pp 241–326
Hussain M, Lee B (1980) A wind tunnel study of the mean pressure forces acting on large groups of low-rise buildings. J Wind Eng Ind Aerodyn 6(3–4):207–225
Janssen W, Blocken B, van Hooff T (2013) Pedestrian wind comfort around buildings: comparison of wind comfort criteria based on whole-flow field data for a complex case study. Build Environ 59:547–562
Kashiwa B (2001) A multi-field model and method for fluid-structure interaction dynamics. Technical report LA-UR-01-1136, Los Alamos National Laboratory, Los Alamos
Kashiwa B, Lewis M, Wilson T (1996) Fluid-structure interaction modeling. Technical report LA-13111-PR, Los Alamos National Laboratory, Los Alamos
Ketzel M, Louka P, Sahm P, Guilloteau E, Sini J, Moussiopoulos N (2000) Intercomparison of numerical urban dispersion models—part II: street canyon in Hannover, Germany. In: 3rd urban air quality conference, Greece
Kim J, Baik J (2010) Effects of street-bottom and building roof heating on flow in three-dimensional street canyons. Adv Atmos Sci 27(3):513–527
Kim JJ, Baik JJ (2004) A numerical study of the effects of ambient wind direction on flow and dispersion in urban street canyons using the rng k-ϵ turbulence model. Atmos Environ 38(19):3039–3048
Kochanski AK, Pardyjak ER, Stoll R, Gowardhan A, Brown MJ, Steenburgh WJ (2015) One-way coupling of the WRF-QUIC urban dispersion modeling system. J Appl Meteorol Clim 54(10):2119–2139

Koutsourakis N, Bartzis J, Markatos N (2012) Evaluation of Reynolds stress, k-ϵ and RNG k-ϵ turbulence models in street canyon flows using various experimental datasets. Environ Fluid Mech 12:379–403

Lilly DK (1992) A proposed modification of the Germano subgrid-scale closure method. Phys Fluids A 4(3):633–636

Liu J, Niu J (2016) CFD simulation of the wind environment around an isolated high-rise building: an evaluation of SRANS, LES and DES models. Build Environ 96:91–106

Meng Q, Berzins M (2014) Scalable large-scale fluid-structure interaction solvers in the uintah framework via hybrid task-based parallelism algorithms. Concurr Comput 26(7):1388–1407

Moonen P, Defraeye T, Dorer V, Blocken B, Carmeliet J (2012) Urban Physics: effect of micro climate on comfort, health and energy demand. Front Arch Res 1:197–228

Munters W, Meneveau C, Meyers J (2016) Turbulent inflow precursor method with time-varying direction for large-eddy simulations and applications to wind farms. Boundary-Layer Meteorol 159(2):305–328

Muñoz-Esparza D, Kosović B, van Beeck J, Mirocha J (2015) A stochastic perturbation method to generate inflow turbulence in large-eddy simulation models: Application to neutrally stratified atmospheric boundary layers. Phys Fluids 27(3):1–27

Murakami S (1997) Current status and future trends in computational wind engineering. J Wind Eng Ind Aerodyn 67:3–34

Murakami S (1998) Overview of turbulence models applied in CWE-1997. J Wind Eng Ind Aerodyn 74–76:1–24

Murakami S, Ooka R, Mochida A, Yoshida S, Kim S (1999) CFD analysis of wind climate from human scale to urban scale. J Wind Eng Ind Aerodyn 81(1–3):57–81

Nelson MA, Addepalli B, Hornsby F, Gowardhan AA, Pardyjak E, Brown MJ (2008) Improvements to a fast-response urban wind model. In: 15th Joint conference on the applications of air pollution meteorology with the AWMA, American Meteor Society, New Orleans, LA, USA, p 5.2

Nelson MA, Brown MJ, Halverson SA, Bieringer PE, Annunzio A, Bieberbach G, Meech S (2016) A case study of the Weather Research and Forecasting Model applied to the Joint Urban 2003 tracer field experiment. Part 2: Gas tracer dispersion. Boundary-Layer Meteorol pp 1–30

Neofytou P, Haakana M, Venetsanos A, Kousa A, Bartzis J, Kukkonen J (2008) Computational fluid dynamics modelling of the pollution dispersion and comparison with measurements in a street canyon in Helsinki. Environ Model Assess 13(3):439–448

Neophytou M, Gowardhan A, Brown M (2011) An inter-comparison of three urban wind models using the Oklahoma City Joint Urban 2003 wind field measurements. J Wind Eng Ind Aerodyn 99(4):357–368

Parker SG (2006) A component-based architecture for parallel multi-physics PDE simulation. Future Gen Comput Sys 22:204–216

Parker SG, Guilkey J, Harman T (2006) A component-based parallel infrastructure for the simulation of fluid-structure interaction. Eng Comput 22:277–292

Poinsot T, Veynante D (2001) Theoretical and numerical combustion. R. T. Edwards Inc., 473 pp

Pol SU, Bagal N, Singh B, Brown M, Pardyjak E (2006) Implementation of a new rooftop recirculation parameterization into the quic fast response urban wind model. In: 6th Conference on Urban environment, American Meteor Society, Atlanta, GA, USA, p JP1.2

Rockle R (1990) Bestimmung der stomungsverhaltnisse im bereich komplexer bebauungsstrukturen. PhD thesis, Vom fachbereich Mechanik, der technischen hochsschule Darmstadt, Germany, 150 pp

Sahm P, Louka P, Ketzel M, Guilloteau E, Sini J (2002) Intercomparison of numerical urban dispersion models—part I: street canyon and single building configurations. Water Air Soil Pollut 2(5–6):587–601

Salim S, Buccolieri R, Chan A, Di Sabatino S (2011) Numerical simulation of atmospheric pollutant dispersion in an urban street canyon: comparison between RANS and LES. J Wind Eng Ind Aerodyn 99(2–3):103–113

Salim S, Ong K (2013) Performance of RANS, URANS and LES in the prediction of airflow and pollutant dispersion. In: Kim HK, Ao S, Rieger BB (eds) IAENG transactions on engineering technologies: Special edition of the world congress on engineering and computer science 2011. Springer Netherlands, Dordrecht, pp 263–274

Santiago J, Martilli A, Martin F (2007) CFD simulation of airflow over a regular array of cubes: part I: three-dimensional simulation of the flow and validation with wind-tunnel measurements. Boundary-Layer Meteorol 122:609–634

Schulman LL, Strimaitis DG, Scire JS (2000) Development and evaluation of the PRIME plume rise and building downwash model. J Air Waste Manag Assoc 50(3):378–390

Seoud R, Vassilicos J (2007) Dissipation and decay of fractal-generated turbulence. Phys Fluids 19:105108

Shishegar N (2013) Street design and urban microclimate: analyzing the effects of street geometry and orientation on airflow and solar access in urban canyons. Clean Energy Tech 1(1):52–56

Singh B, Hansen BS, Brown MJ, Pardyjak ER (2008) Evaluation of the QUIC-URB fast response urban wind model for a cubical building array and wide building street canyon. Environ Fluid Mech 8(4):281–312
Singh M, Laefer D (2015) Recent trends and remaining limitations in urban microclimate models. Open Urban Studies Demog J 1:1–12
Souch C, Grimmond S (2006) Applied climatology: urban climate program. Phys Geogr 30:270–279
Tabor G, Baba-Ahmadi M (2010) Inlet conditions for large eddy simulation: a review. Comput Fluids 39:553–567
Tinarelli G, Brusasca G, Oldrini O, Anfossi D, Castelli ST, Moussafir J (2007) Micro-Swift-Spray (MSS): a new modeling system for the simulation of dispersion at microscale. General description and validation. In: Borrego C, Norman AL (eds) Air pollution modeling and its application XVII. Springer US, Boston MA, pp 449–458
Tominaga Y, Stathopoulos T (2009) Numerical simulation of dispersion around an isolated cubic building: comparison of various types of k-ϵ models. Atmos Environ 43(20):3200–3210
Tominaga Y, Stathopoulos T (2010) Numerical simulation of dispersion around an isolated cubic building: model evaluation of RANS and LES. Build Environ 45(10):2231–2239
Tominaga Y, Stathopoulos T (2011) CFD modeling of pollution dispersion in a street canyon: comparison between LES and RANS. J Wind Eng Ind Aerodyn 99(4):340–348
Tominaga Y, Mochida A, Murakami S, Sawaki S (2008) Comparison of various revised k-ϵ models and les applied to flow around a high-rise building model with 1:1:2 shape placed within the surface boundary layer. J Wind Eng Ind Aerodyn 96(4):389–411
Toparlar Y, Blocken B, Vos P, Heijst G, Janssen W, Hooff T (2015) CFD simulation and validation of urban microclimate: a case study for Bergpolder Zuid, Rotterdam. Build Environ 83:79–90
Uehara K, Murakami S, Oikawa S, Wakamatsu S (2000) Wind tunnel experiments on how thermal stratification affects flow in and above urban street canyons. Atmos Environ 34:1553–1562
Valente P, Vassilicos J (2011) The decay of turbulence generated by a class of multi-scale grids. J Fluid Mech 687:300–340
Versteeg H, Malalasekera W (1995) An introduction to computational fluid dynamics: the finite volume method, 1st edn. Longman Scientific & Technical, Essex, 257 pp
Warner S, Platt N, Heagy JF, Jordan JE, Bieberbach G (2006) Comparisons of transport and dispersion model predictions of the mock urban setting test field experiment. J Appl Meteorol Clim 45(10):1414–1428
Weinkauf T, Theisel H, Gelder AV, Pang A (2011) Stable feature flow fields. IEEE Trans Vis Comput Graph 17(6):770–780
Wilcox DC (2006) Turbulence modeling for CFD, 3rd edn. DCW Industries Inc., La Canada, 522 pp
Wilson DJ (1979) Flow pattern over flat-roofed buildings and application to exhaust stack design. ASHRAE 85:284–295
Wu H, Kriksic F (2012) Designing for pedestrian comfort in response to local climate. J Wind Eng Ind Aerodyn 104–106:397–407
Xia Y (2006) Computational modeling for large deformation fluid structure interaction problems. PhD thesis, Department of Mechanical Engineering, University of Utah, USA, 292 pp
Xie X, Huang Z, Wang J (2005) Impact of building configuration on air quality in street canyons. Atmos Environ 39:4519–4530
Yang XIA, Meneveau C (2016) Recycling inflow method for simulations of spatially evolving turbulent boundary layers over rough surfaces. J Turb 17(1):75–93